https://doi.org/10.5194/hess-2023-84
Preprint. Discussion started: 8 May 2023

Hydrology and Earth System Sciences
Discussions

Shannon Entropy of Transport Self-Organization Due to Dissolution/Precipitation Reaction at Varying Peclet Number in an Initially Homogeneous Porous Media

Evgeny Shavelzon[1] and Yaniv Edery[2]
[1,2]Technion – Israel Institute of Technology, Haifa, Israel
Correspondence: Yaniv Edery (yanivedery@technion.ac.il)

Abstract. Dissolution and precipitation processes in reactive transport in porous media are ubiquitous in a multitude of contexts within the field of Earth sciences. In particular, the dynamic coupling between the reactive precipitation / dissolution processes and the solute transport is of interest, as it is capable of giving rise to the emergence of preferential flow paths in the porous host matrix. This coupling is critical to a variety of Earth science scenarios, although the approaches to its characterization remain disputed. It has been shown that the emergence of preferential flow paths can be considered a manifestation of transport self-organization in porous media, as they create spatial gradients that distance the system from the state of perfect mixing and allow for a faster and more efficient fluid transport through the host matrix. To investigate the dynamic feedback between the transport and the reactive process in the field and its influence on the emergence of transport self-organization, we consider a two-dimensional Darcy-scale formulation of a reactive transport setup, where the precipitation and dissolution of the host matrix are driven by the injection of an acid compound, establishing local equilibrium with the resident fluid and an initially homogeneous porous matrix, composed of a calcite mineral. The coupled reactive process is simulated in a series of computational analyses employing the Lagrangian particle tracking (LPT) approach, capable of capturing the subtleties of the multiple scale heterogeneity phenomena. As the reactive process evolves, the dissolution / precipitation reactions are allowed to affect the local values of porosity and hydraulic conductivity in the host matrix, thus creating a dynamic feedback in the system. Subsequently, we employ computational non-reactive tracer tests to obtain the solute concentration data in the field, used to calculate the Shannon entropy of the transport. We employ the Shannon entropy to quantify the emergence of self-organization in the field, which we define as a relative reduction in entropy, compared to its maximum value. Our findings show that transport self-organization in an initially homogeneous field increases with time, along with the emergence of the field heterogeneity due to the interplay between transport and reactive process. By studying the influence of the transport Peclet number on the reactive process, we arrive at a conclusion that self-organization is more pronounced in diffusion-dominated flows, characterized by small Peclet values. The explanation for this lies in the fact that in a completely homogeneous field, the dominant mechanism to drive reactive components out of equilibrium is the stochasticity of diffusion. The self-organization of the breakthrough curve exhibits the opposite tendencies, that are explained from the thermodynamic perspective. The hydraulic power, required to maintain the driving head pressure difference between inlet and outlet, increases with the increasing variance of the hydraulic conductivity in the field due to the evolution of the reactive process in the field. This increase in

https://doi.org/10.5194/hess-2023-84
Preprint. Discussion started: 8 May 2023


Hydrology and Earth System Sciences
Discussions

power, supplied to the fluid traveling in the porous medium, results in an increase in the level of transport self-organization in the medium.

1 Introduction

1.1 Dissolution/precipitation reaction and preferential flow paths in porous media

Dissolution and precipitation processes in reactive transport in porous media play an important role in multiple contexts in the field of Earth sciences, such as geological CO_2 storage [Ajayi et al. (2014)], reactive contaminant transport [Brusseau (1994)], and acid injection in petroleum reservoirs [Shazly (2021)]. They are responsible for alteration of the transport characteristics of the porous media and emergence of preferential flow paths [Singurindy and Berkowitz (2003), Al-Khulaifi et al. (2017)], as dissolution / precipitation reactive processes lead to changes in the dimensions of the pores and their connectivity, thus introducing coupling between the chemical reaction and the transport in the media. This is observed, for example, in reactive infiltration in a porous medium, where chemical reaction at the solid-fluid interface causes dissolution of the surrounding porous matrix, creating nonlinear feedback mechanisms that often lead to greatly enhanced permeability [Ladd and Szymczak (2021), Szymczak and Ladd (2006)]. The solid-fluid interface instability, observed in this case, is similar to the viscous fingering phenomenon in the field of multi-phase flow, with undulation areas formed first at the solid-fluid interface of the porous media due to dissolution, which are later transformed into well-defined finger-like channels or wormholes, that rapidly advance into the medium. As dissolution proceeds, these fingers interact, competing for the available flow.

These wormholes that funnel the flow can be regarded as preferential flow paths, ubiquitous in heterogeneous porous media, where most of the transport is concentrated. The importance of preferential flows in determining the transport properties of the porous media is widely recognized, as they allow rapid solute transport and alter residence times [Beven and Germann (1982), Stamm et al. (1998), Radolinski et al. (2022), Edery et al. (2014), Edery et al. (2016a)]. As these preferential flow align with the average flow direction, they introduce solute concentration gradients in the direction transverse to flow [Zehe et al. (2021)] and an increasingly non-Fickian transport behavior, thus requiring a global homogenization approach for transport characterization that considers these subtleties in the upscaling / volume averaging methods. The formation of preferential flow paths in the porous matrix due to interaction between dissolution reaction and transport processes has been reported in a multitude of experimental studies [Kamolpornwijita et al. (2003), Zhang et al. (2021), Snippe et al. (2020), Li et al. (2019)], while the opposite scenario of a precipitation reaction, such as in the formation of carbonate deposits during CO_2 sequestration, was investigated by Yan et al. (2020); they reported clogging of pores, leading to alteration or complete blockade of the preferential flow paths. As opposed to the case of highly conductive networks, such as fractured rock formations, the preferential flow paths in the saturated heterogeneous porous media are not always well defined. For this case, Zehe et al. (2021) have reported that a higher variance in the hydraulic conductivity field leads to the intensification of the preferential flow path phenomenon via a stronger concentration of solute within a smaller number of paths. Changing the observing perspective, [Berkowitz and Zehe (2020)] have argued that the emergence of preferential flow paths can be viewed as a manifestation of self-organization, as the

https://doi.org/10.5194/hess-2023-84
Preprint. Discussion started: 8 May 2023


Hydrology and Earth System Sciences
Discussions

spatial concentration gradients, created within the system, distance the system from the state of perfect mixing, thus allowing for a faster and more efficient fluid transport.

1.2 Self-organization in physical systems and thermodynamic framework

The findings discussed above have brought us closer to classification of the emerging preferential flow paths in reactive transport in porous media as an embodiment of self-organization. Before addressing the specific problem of the emergence of preferential flow paths, it is in order to first discuss some basic concepts related to the phenomenon of self-organization in physical systems. Self-organization refers to a broad range of pattern-formation processes, occurring through interactions internal to the system, without intervention by external directing influences [Camazine et al. (2001)]. Examples of self-organization in physical systems include formation of patterns in chemical reactions [Turing (1952)], animal behavior, such as bird flocking [Hemelrijk and Hildenbrandt (2012)] and river network formation [Stolum (1996)]. In this context, it is interesting to consider reaction-diffusion systems, that have attracted much interest as a prototype model for pattern formation in nature. An attempt to provide an explanation of morphogenesis in the field of mathematical biology was first made by Alan Turing [Turing (1952)], that proposed a model based on chemical reaction-diffusion interaction, where two homogeneously distributed substances interact to produce stable stationary patterns, represented by concentration deviations of the two substances inside the domain of the reaction. The reaction is autocatalytic and is represented by a system of nonlinear differential equations, thus possessing the capability for exhibiting self-organizing modes. The necessary condition for pattern emergence requires that diffusion coefficients of both substances differ, otherwise no self-organization will take place. This feature counteracts the homogenizing action of diffusion. Turning to the field of hydrology, Berkowitz and Zehe (2020) have stated that, while self-organization in well-defined networks, such as rivers, is clearly distinguishable, nevertheless also the cases that lack well-defined network, such as transport in heterogeneous groundwater systems in the absence of fractures, are capable of displaying some characteristics of self-organization, that is manifested through spatially correlated, anisotropic patterns of structural and hydraulic properties.

Within the thermodynamic framework, Haken (1983) has defined self-organization as an emergence of ordered macroscale states in an open, complex system, far from thermodynamic equilibrium due to exchange of energy and matter with surroundings, as a result of a synergetic interplay of microscale, irreversible processes. Recall the definition of entropy by Boltzmann, that is directly related to the number of possible microstates of a system that are consistent with a given macrostate, characterized by the macroscopic thermodynamic properties of the system [Haken (1983)]. An ordered state is characterized by the reduction in entropy of the system, compared to its maximum value at equilibrium, thus, a macrostate with a lesser amount of corresponding possible microstates is considered more ordered [Kondepudi and Prigogine (1998)]. Since, according to the 2nd law of Thermodynamics, the overall entropy of the system and its surroundings cannot decrease, this reduction in entropy has to be exported from the system to surroundings to establish an ordered state. The export of entropy from the system requires that physical work is performed on the system in order to maintain the current level of self-organization. One of the most exciting examples that come to mind to illustrate this concept is biological life. Erwin Schrodinger in his highly influential book *What is Life?* [Schrodinger (1944)] describes a living organism as a non-equilibrium thermodynamic system in interaction with its

https://doi.org/10.5194/hess-2023-84
Preprint. Discussion started: 8 May 2023


Hydrology and Earth System Sciences
Discussions

surroundings, that maintains a level of inner self-organization. How does a living organism manage to avoid decay into the inert state of equilibrium? The answer is simple: by consuming food and transforming it into energy through metabolic processes. This energy allows the organism to maintain its level of self-organization by exporting the entropy, produced by irreversible physiological processes, to the surroundings. In other words, in order to maintain self-organization within a living organism, it works to decrease the level of self-organization of its surroundings by exporting entropy outside.

While the thermodynamic framework refers to physical entropy, introduced by [Clausius (1857)], the information entropy, first defined by [Shannon (1948)], has proven to be extremely useful in quantifying self-organization in various fields of physical science. This parameter, also referred to as the Shannon entropy, was introduced originally in the framework of communication. Viewing communication as a statistical process, Shannon employed an entropy-like parameter, defined similarly to Boltzmann's definition of entropy, to provide a measure for the amount of transmitted information, carried by a certain sequence of symbols. The applications of Shannon entropy in the field of geophysical science are plenty; Chiogna and Rolle (2017) have employed Shannon entropy to quantify dilution and reactive mixing in solute transport problems; Schweizer et al. (2017) used it for uncertainty assessment in complex geological models; Mays et al. (2002) have measured temporal and spatial complexity of unsaturated flow in heterogeneous media; Woodbury and Ulrych (1996) have applied the minimum relative entropy principle (MRE) from the field of information theory to the problem of recovering the release history of a groundwater contaminant; Zehe et al. (2021) has studied self-organization in preferential flow paths in porous media of various degrees of spatial heterogeneity and quantified it in terms of Shannon entropy. They found that stronger transversal concentration gradients emerge with an increasing variance of the hydraulic conductivity field, which is reflected in a smaller entropy of the transversal distribution of transport pathways. Their findings suggest that a higher variance of the hydraulic conductivity field coincides with stronger self-organization of transport pathways (represented by steepening of the concentration gradient in the direction transverse to flow). The explanation to this non-intuitive finding is given in terms of energy: in the thermodynamic framework, the emergence of spatial self-organization requires energy input into the system, which grows along with the increase in the level of self-organization. Since the energy input in the form of hydraulic power, necessary to sustain steady-state fluid flow and tracer transport, grows with the variance of the hydraulic conductivity field, this enables an increase in self-organization of the transport in the field.

1.3 Lagrangian particle approach in transport in porous media

Among the family of numerical methods employed to simulate transport and reaction problems in porous media, the Lagrangian particle approach continues to gain more prominence in the recent decades, along with the continuing development of powerful computers [Jiao et al. (2021), Sole-Mari and Fernandez-Garcia (2018), Sole-Mari et al. (2020)]. The Lagrangian family of computational methods considers the fluid phase as consisting of discrete particles and tracks the path of each particle, as opposed to the more conventional Eulerian family of methods, where the fluid phase is treated as a continuum and its governing equations are developed based on conservation principles [Zhang and Chen (2007), Meakin and Tartakovsky (2009)]. In the Lagrangian approach, motion and interaction of particles are defined by a specific set of laws that correspond to

https://doi.org/10.5194/hess-2023-84
Preprint. Discussion started: 8 May 2023


Hydrology and Earth System Sciences
Discussions

the physical situation of interest. Statistical analysis is then applied to the particle trajectories and interactions. The Lagrangian particle methods are not susceptible to numerical instabilities that are often present in the numerical simulations where an Eulerian approach is employed [Meakin and Tartakovsky (2009)]. Perez et al. (2019) employed random walk particle tracking to simulate bimolecular irreversible chemical reaction in porous media and have shown the equivalence of their formulation to the well-known advection-diffusion-reaction equation (ADRE), while others used it to simulate reactive transport in heterogeneous fields that displays non-Fickian behavior [Berkowitz et al. (2013), Edery et al. (2013), Edery et al. (2010), Edery et al. (2009), Edery et al. (2016b)]. Other applications of Lagrangian methods include particle dispersion in fluid [Shirolkar et al. (1996)], multiphase flows [Meakin and Tartakovsky (2009)], reactive transport [Schmidt et al. (2019)] and impact problems, such as water impingement on a surface [Petrosino et al. (2021)].

1.4 Objectives

To investigate the dynamic coupling between the transport and the reactive process in an initially homogeneous porous medium and its influence on the emergence of transport self-organization in the medium, we consider a two-dimensional Darcy-scale formulation of a reactive transport setup, where precipitation and dissolution in the medium are driven by the injection of an acid compound, establishing local equilibrium with the resident fluid and an initially homogeneous porous medium, composed of calcite mineral. The coupled reactive process is simulated in a series of computational analyses where the low pH water is injected into an initially homogeneous domain, at first in equilibrium with the resident fluid (high pH water). We employ a Lagrangian particle tracking (LPT) approach, capable of capturing the subtleties of the multiple scale heterogeneity phenomena, along the lines of Edery et al. (2021).

In particular, we are interested in the influence of the transport Peclet number on the reactive process and the emergence of self-organization of the transport in the porous medium. To investigate this relation, we simulate a number of reactive transport scenarios for different values of advective to diffusive transport rates, characterized by the Peclet number. This is achieved by applying different values of the inlet-outlet hydraulic pressure head drop boundary condition to the field. We employ Shannon entropy along the lines of Zehe et al. (2021) to quantify the emergence of transport self-organization in the medium. In Section 2 we review the basic methodology of our reactive setup approach, followed by the discussion of the concept of self-organization in the context of transport in porous medium, its quantification and relation to hydraulic power in Section 3. We present and discuss the obtained results in section 4.

2 Reaction, flow and transport modelling

2.1 Chemical reaction model

The key component in dissolution-precipitation reactions is the stoichiometric equilibrium between the reactants. In the system under investigation, the simulated reactive transport scenario is that of an injected acid compound (low pH water), establishing

https://doi.org/10.5194/hess-2023-84
Preprint. Discussion started: 8 May 2023


Hydrology and Earth System Sciences
Discussions

local equilibrium with the resident fluid (high pH water) and the porous medium, composed of a calcite mineral. This fairly common setting in the field of geosciences constitutes a specific case of Edery et al. (2011), where dedolomitization is also included in the chemical model (see also Singurindy and Berkowitz (2003), Al-Khulaifi et al. (2017)). When the low pH water (pH level of 3.5) enters the calcite porous medium, initially saturated and in chemical equilibrium with the resident fluid (pH level of 8), dissolution of calcite occurs, accompanied by the production of calcium and carbonic acid. For pH values below 8, the equilibrium reaction is represented by the following equations

$$CaCO_3 + H^+ \leftrightarrow Ca_2^+ + HCO_3^- \tag{1}$$

$$HCO_3^- + H^+ \leftrightarrow H_2CO_3 \tag{2}$$

Another chemical equilibrium is possible for higher pH values, where the deprotonation of carbonic acid produces CO_3^{2-}. However, this reaction is neglected in the present study as the fluid pH level is assumed to be bounded by that of the resident fluid (see Edery et al. (2011) for details). The reaction is assumed to be fully reversible, therefore the opposite precipitation reaction is also possible, given that the pH conditions are favorable. Combining both equations and assuming abundance of calcium and calcite in the domain of interest along the lines of Edery et al. (2021), we obtain the following simplified equation

$$A \leftrightarrow B \tag{3}$$

where A and B represent $2H^+$ and H_2CO_3, respectively. The direction of reaction is governed by the deviation from the chemical equilibrium, as defined by the current concentrations of H^+ and H_2CO_3 in the specific area of reaction. In the presence of H^+ concentration above the equilibrium value, dissolution will occur and vice versa. While pH levels control the dissolution-precipitation reaction, the proton concentration that establishes the pH is controlled by the transport and diffusion of the invading fluid.

2.2 Flow and transport simulation

To investigate the dynamic coupling between the transport and reactive processes in the porous medium, we consider a two-dimensional field of dimensions 12×30 cm^2, made of calcite mineral. The field is assumed to be fully saturated with a resident high pH water and initially in chemical equilibrium. Low pH water is being injected at the inlet boundary, causing reaction inside the porous medium as it advances. The field is discretized into $N_x \times N_y$ computational cells, where $N_x = 150$ and $N_y = 60$ are the number of cells in the direction parallel and transverse to the flow, respectively, each cell having dimensions of $\Delta x, \Delta y = 0.2$ cm. The field is initially homogeneous in terms of hydraulic conductivity K and porosity θ that have initial values of $K_0 = 10.9869$ cm/min and $\theta_0 = 0.4$, respectively. A hydraulic head drop boundary condition Δh is applied between the field's inlet and outlet boundaries, while the upper and lower field boundaries are ideal (reflective) walls. The flow within the field, subject to the boundary conditions as described above, is governed by the continuity and the Darcy equations (4-5) and solved in terms of the hydraulic pressure head with the help of a Finite element method computer code (Guadagnini and

https://doi.org/10.5194/hess-2023-84
Preprint. Discussion started: 8 May 2023


Hydrology and Earth System Sciences
Discussions

Neuman (1999)). The obtained hydraulic head field is then converted into flow velocity at each computational cell.

$$\nabla \cdot \mathbf{q}(\mathbf{x}) = 0 \tag{4}$$

$$\mathbf{q}(\mathbf{x}) = -K\nabla h(\mathbf{x}) \tag{5}$$

Here $\mathbf{q}$ and h are the Darcy flux and the hydraulic head distributions over the field and K is the hydraulic conductivity, all functions of the field spatial coordinate $\mathbf{x}$. Here and throughout the paper bold font is used to specify vector fields, as opposed to scalar fields written in the regular font.

The solute transport across the field is simulated using a Lagrangian particle tracking approach (Le Borgne et al. (2008)). The invading fluid is represented by the reactive A particles injected into the porous medium. A total number of $N_{tot} = 5e5$ A particles, representing the available pore volume in the field at pH 3.5, is injected per pore volume time at the inlet boundary at a constant rate proportional to the mean flow velocity in the initial homogeneous field, so that in every computational time step Δt the amount of injected particles is $v_0 \cdot (\Delta t/L) \cdot N_{tot}$, where L is the domain length in the direction of the flow and v_0 is the mean flow velocity magnitude within the initial homogeneous field (assuming that the change in the mean conductivity value is minor over the simulation time). The mean velocity v_0 is calculated from the applied pressure head drop over the field Δh using Darcy's law: $v_0 = K_0/\theta_0 \cdot \Delta h/L$. The particles injected at each time step are flux-weighted according to the conductivity distribution of the inlet cells. The particle injection rate is such that all of the available pore volume in the field is sampled by the particles by the time all N_{tot} of them have been injected. The time of this occurrence will be referred to as pore volume time T_{pv} throughout the paper.

The injected A particles are being advanced in the field using the Langevin equation, that combines deterministic (advective) and stochastic (diffusive) contributions [Risken (1996)]. The position $\mathbf{d}(t)$ of a particle due to the combined effect of advective and diffusive transport mechanisms is described by (6), where $\mathbf{v}$ is the flow velocity field, t is the computational time, D is the diffusion coefficient of the invading fluid in the porous medium and $\boldsymbol{\xi}(t)$ is a vectorial Gaussian random variable characterized by $\langle \boldsymbol{\xi}(t) \rangle = \mathbf{0}$ and $\langle \xi_i(t)\xi_j(t') \rangle = \delta_{ij}\delta(t-t')$.

$$\frac{d\mathbf{d}(t)}{dt} = \mathbf{v}[\mathbf{d}(t)] + \sqrt{2D}\boldsymbol{\xi}(t) \tag{6}$$

An important property of Langevin equation (6) is its equivalence to the well-known advection-diffusion equation (ADE) [Risken (1996), Perez et al. (2019)]. To be used in the context of a numerical simulation, the equation is discretized using the simple Euler-Maruyama method [Kloeden (1992)] as follows

$$\mathbf{d}_{k+1} = \mathbf{v}_k \cdot \Delta t + \mathbf{d}_D \tag{7}$$

where $\mathbf{d}_{k+1} = \mathbf{d}(t_{k+1})$ is the particle location at the current computational time step $t_{k+1} = \Delta t \cdot (k+1)$ and $\mathbf{v}_k = \mathbf{v}[\mathbf{d}(t_k)]$ is the flow velocity at the particle location at the previous computational time step $t_k = \Delta t \cdot k$ (here the index k is not to be confused with the hydraulic conductivity K). The diffusive contribution is given by $\mathbf{d}_D = \sqrt{2D\delta t} \cdot N(0,1)$, where D=1e-5

https://doi.org/10.5194/hess-2023-84
Preprint. Discussion started: 8 May 2023

Hydrology and Earth System Sciences
Discussions

cm^2/min is the representative value of the diffusion coefficient [Domenico and Schwartz (1997)], $N(0,1)$ is a standard normally distributed random variable and $\delta t = \delta s/v$ is the time it takes a particle to move the fixed distance $\delta s = \Delta x/10$ while traveling with the flow at a speed of magnitude $v = |\mathbf{v}|$. The obtained diffusive contribution has no spatial preference, since its spatial direction is represented by a uniformly distributed random variable between $[0, 2\pi]$. The particle movement in the duration of the computational time step Δt consists of a series of jumps of a constant magnitude δs, to which the diffusive contribution is added. This series of jumps continues until their cumulative time $\sum_i \delta t_i$, where *i* is the jump index in the series, reaches Δt.

At first, no B particles exist in the field. After all newly injected A particles have been advanced to their current locations, they are allowed to react according to an algorithm described in Section 2.3. Following reaction, as described by (3), B particles appear in the field and the computational cell values of porosity and hydraulic conductivity in the area of reaction are being updated correspondingly, thus creating a coupling between the reactive and the transport processes. Beginning the next computational step Δt, another set of A particles is being injected into the field employing flux-weighting in accordance to the reaction-modified conductivity distribution of the inlet cells. Then, all available particles in the field (both A and B) are being advanced again and reaction occurs. Note that the diffusive contribution to particle displacement $\mathbf{d}_D$ allows for the mixing effect in the field due to its stochastic nature. Following the changes in the hydraulic conductivity field due to the reactive process, the pressure field and the corresponding flow velocity field are updated at constant time intervals of $10\Delta t$ (in order to reduce constraints associated with computational costs), while the reaction is allowed to occur every Δt. The simulation continues until the pore volume time T_{pv} is reached, while the A particles injection rate remains constant throughout the simulation. Hydraulic conductivity, pressure head, porosity and velocity fields, as well as the amount of dissolution-precipitation reactions that took place in each computational cell, are recorded at constant time intervals of $10\Delta t$ as well, to be analyzed in the post-processing stage. The particle transport algorithm, along with the chemical reaction model described above, constitute two important aspects of the kinetic reaction mechanism, as implemented in the current study.

2.3 Kinetic reaction mechanism

In the system under investigation, the kinetic reactive process operates accordingly to an algorithm, developed to mimic the actual chemical dissolution/precipitation reactions that take place in practice. After all existing A and B particles in the field have been advanced in the current time step, reaction is allowed to occur. Since the reaction is assumed to be locally instantaneous, at each instant of computational time Δt the reaction is allowed to proceed until local equilibrium is reached in each field cell. For that purpose, the number of currently residing particles of both kinds is assessed in each cell. Each A particle is assigned a molar amount based on the assumption that the total number of A particles injected per pore volume time N_{tot}, distributed evenly across the field, result in the pH level of 3.5 throughout the field, which corresponds to the pH level of the invading fluid. The following calculation is performed: a total available pore volume in the computational field $\theta_0(N_x\Delta x)(N_y\Delta y)$ is multiplied by the molar density of the hydrogen ions that are being injected into the field, corresponding to a pH level of 3.5. This gives 4.55e-5 mol of hydrogen ions that are required to fill the initially available pore volume to obtain a pH level of 3.5

https://doi.org/10.5194/hess-2023-84
Preprint. Discussion started: 8 May 2023


Hydrology and Earth System Sciences
Discussions

throughout the field. To obtain the molar amount assigned to a single A particle, this value is divided by N_{tot}. For $N_{tot} = 5e5$ A particles as defined in the current simulation, each one obtains a parcel of 9.1e-11 mol of H^+. Based on (3), each B particle obtains an identical amount of moles of carbonic acid. The number of A particles in a particular cell to obtain pH 3.5 there is calculated by dividing N_{tot} particles by the number of computational cells in the field $N_x \cdot N_y$ to obtain approximately 56 (while zero A particles in a cell represents pH level of 8 there, which correponds to the pH of the resident fluid). Based on the actual number of A particles in the cell, the current pH level there is estimated using a linear proportion from these limiting values. The equilibrium value of the fractional amount of H_2CO_3 in relation to the total amount of carbonates in a cell, denoted by $\alpha_1(pH)$, is calculated based on the current pH value in the cell as

$$\alpha_1(pH) = \frac{10^{-2pH}}{10^{-2pH} + 10^{-pk_{a1}} + 10^{-pk_{a2}} + 10^{-pH-pk_{a1}}} \tag{8}$$

with the standard values $pk_{a1} = 6.35, pk_{a2} = 10.33$ [Manahan (2000)] (see Appendix A in Edery et al. (2011) for details). The value of $\alpha_1(pH)$ is then compared to the current fractional amount of H_2CO_3 in a cell, calculated based on an assumption that the total amount of carbonates in a cell at any time corresponds to the amount of H^+ that results in a pH level of 3.5 there. The direction of the reaction may now be determined in accordance with (3): dissolution will occur if the fractional amount of H_2CO_3 is smaller than the equilibrium value, and vice versa. A single reaction is allowed to occur, during which a single A particle in a cell transforms into a B particle or vice versa. After each reaction turn, the local pH level in a cell and the fractional amount of H_2CO_3 there in equilibrium $\alpha_1(pH)$ and in practise are recalculated and the reaction process is repeated until convergence to equilibrium is reached.

After that, the cell porosity θ is updated in accordance with (9), where the subscripts $k+1$ and k denote values at the current and previous computational steps, respectively (before and after the reaction has taken place). Here, the porosity increment is actually the volume of calcite, dissolved or precipitated due to reaction, divided by the volume of the cell $\Delta x \Delta y$ (assuming unit cell depth). The change in cell volume is equal to the change in molar amount of H_2CO_3 due to reaction in the cell $d[H_2CO_3]$ (can be positive or negative, depending on the direction of reaction) times the molar volume of calcite, taken to be $M_{CaCO_3} =$ 36.93 cm^3/mol [Morse and Mackenzie (1990)]. The porosity is not allowed to exceed limiting values of 0.01 and 0.99, set to avoid occurrence of non-physical scenarios. The hydraulic conductivity K is then updated employing the Kozeny-Carman relation (10).

$$\theta_{k+1} = \theta_k + \frac{d[H_2CO_3]M_{CaCO_3}}{\Delta x \Delta y} \tag{9}$$

$$K_{k+1} = K_k \cdot \frac{\theta_{k+1}^3}{(1-\theta_{k+1})^2} \cdot \frac{(1-\theta_k)^2}{\theta_k^3} \tag{10}$$

This process is repeated for each of the cells in the field before the particles are allowed to advance again in the next computational time step. In order to reduce constraints, associated with computational costs, reaction enhancement has also been considered. For this purpose, the molar amount of H^+ associated with each injected A particle is increased by several orders

https://doi.org/10.5194/hess-2023-84
Preprint. Discussion started: 8 May 2023


Hydrology and Earth System Sciences
Discussions

of magnitude. This is equivalent to accelerating the reactive process in the field, while the overall dynamics, associated with the reactive process, remains the same.

2.4 Definition of the Peclet number

The Peclet number plays an important role in our reactive system. As a usual practice, Peclet number is calculated based on an Eulerian length scale, such as the mean grain or pore diameter in the pore scale simulation or the characteristic correlation length of the heterogeneous porous media for the case of the Darcy scale simulation [Nguyen and Papavassiliou (2020)]. The Eulerian definition of the Peclet number as the ratio of advective to diffusive transport rates gives the following well-known relation $Pe = \tilde{v}L/D$, where $\tilde{v}$ is the mean velocity and L is the characteristic length. This definition often yields estimates that allow little physical insight on the subject of the relative contributions of the advective and diffusive processes in the transport in porous media under investigation. Moreover, in the case of reactive transport in an initially homogeneous porous medium on the Darcy scale, such as in the current study, where heterogeneity is gradually introduced in the field, correlation length is time-dependent; this calls for alternative approaches in defining the Peclet number, capable of giving a deeper insight into the transport characteristics. In order to find a meaningful estimate for this parameter, we attempt at formulating the expression for the Peclet number based on Lagrangian length scale quantities, noting, after Nguyen and Papavassiliou (2020), that the nature of hydrodynamic dispersion is Lagrangian. For this purpose we turn to the Langevin equation (6), which governs the particle advancement in the simulation. Each jump made by a particle during the time period δt consists of a constant value advective contribution $\delta s = \Delta x/10$ and a diffusive contribution $\sqrt{2\,D\,\delta t}\cdot N(0,1)$ (see Section 2.2). Only the magnitude of the diffusive contribution is of importance, therefore we will consider its absolute value $\sqrt{2\,D\,\delta t}\cdot|N(0,1)|$. The random variable $|N(0,1)|$ is half-normally distributed with expectation value of $\sqrt{(\frac{2}{\pi})}$ [Leone et al. (1961)]. Therefore, we are able to formulate the expression for the Peclet number directly from its definition as the ratio of advective to diffusive transport rates, given by $Pe = \delta s/\sqrt{4/\pi\,D\,\delta t}$. The time duration of a single jump is determined as $\delta t = \delta s/v$, where v is the magnitude of the fluid velocity at the current particle location. Assuming that the change in the mean conductivity value is minor over the simulation time, we can replace v with the initial flow velocity $v_0 = K_0/\theta_0\cdot\Delta h/L$. Thus, we finally obtain the expression for the transport Peclet number in our simulation

$$Pe = \sqrt{\frac{\pi\delta s\,K_0\,\Delta h}{4\,D\,L\,\theta_0}} \tag{11}$$

The above definition provides a direct estimate of the relative contributions of the advective and diffusive processes in the transport in porous media. This approach may prove useful for Lagrange particle tracking methods where the advective and diffusive transport contributions are defined explicitly.

To investigate the influence of the Peclet number of the transport on the evolution of the reactive process and the emergence of transport self-organization in the field, we simulate a number of reactive transport scenarios for different values of the Peclet number. This is achieved by applying different values of the inlet-outlet hydraulic head drop boundary condition Δh. The computational time step Δt is correlated with Δh in such a way that in each simulated reactive transport scenario,

https://doi.org/10.5194/hess-2023-84
Preprint. Discussion started: 8 May 2023


Hydrology and Earth System Sciences
Discussions

corresponding to a specific value of Δh, an equal number of 1800 time steps and, correspondingly, reaction events occur per pore volume time T_{pv}.

3 Identifying and quantifying self-organization

3.1 Emergence of transport self-organization in reactive transport in an initially homogeneous porous media

The computational setting described in the previous section mimics the dynamics of a coupled dissolution-precipitation reactive process in a calcite porous medium, leading to an emergence of heterogeneity in an initially homogeneous field. Previous studies have shown that self-organization of the solute transport in the field is expected to emerge in such a situation in the form of preferential flow paths that lead to solute concentration gradients in the direction transverse to flow [Zehe et al. (2021)], yet the details of this self-organization emergence and evolution are critical to understanding the large-scale dynamics of the coupled reactive process in the field. Along the lines of Section 1.2, we argue that organized states, characterized by reduced entropy, can emerge in an open system, driven away from equilibrium due to exchange of energy or matter with surroundings. Such a system may persist in a stationary nonequilibrium state. Since, according to the second law, overall entropy cannot decrease, in such a case entropy must be exported from the system to its surroundings.

Appendix A presents a simple heat transfer example that illustrates how an open thermodynamic system can be maintained in a stationary nonequilibrium state through an inflow of energy. Following the same concept, one can generalize this finding to the system under investigation where the transport self-organization in the field in terms of the emergence of preferential flow paths is the outcome of the coupled reactive process that introduces heterogeneity in an initially homogeneous field. In our system, energy influx occurs in the form of hydraulic power, supplied to the flow to overcome the hydraulic resistance of the field by the applied hydraulic pressure head drop boundary condition. Such a system may persist in a nonequilibrium stationary state, characterized by the lowered entropy of the transversal distribution of solute concentration, with the energy - matter influx acting against depletion of transversal concentration gradients. For our system, an equilibrium state corresponds to the state of perfect mixing in the field, where no such gradients exist [Zehe et al. (2021)].

To analyze the emergence of self-organization in our computational field, we consider snapshots of the field in terms of hydraulic conductivity, taken at different computational times as the reactive process in the field evolves. We consider each snapshot as a thermodynamic system and perform a non-reactive tracer test by injecting non-reactive solute at the field's inlet. To identify the driving mechanism that leads to an emergence of heterogeneity in an initially homogeneous porous medium, followed by self-organization of the transport in the field, let us consider two limiting cases related to the nature of the transport mechanism in the field, as applicable to our reactive transport setting, described in Section 2. First, we consider a case when no advection is present (the advective velocity $v = 0$). In this scenario, reactive A particles advance within the field due to diffusive action only. Because of the stochastic nature of the diffusive process that lacks spatial preference, and since the diffusive properties of the reactant and the product solutes are identical (also, in our model diffusion is independent of poros-

https://doi.org/10.5194/hess-2023-84
Preprint. Discussion started: 8 May 2023


Hydrology and Earth System Sciences
Discussions
Open Access
EGU

ity), we expect that the dissolution and precipitation reactions will occur uniformly in space, thus the conductivity field will remain approximately homogeneous in the direction transverse to flow. Therefore, we suggest that in the absence of advection no mechanism exists in our reactive setup to create heterogeneity in the field and no transport self-organization will take place in that case. In the opposite limiting case when no diffusion is present (the diffusion coefficient $D = 0$), a dissolution reaction will first take place uniformly at the inlet of the initially homogeneous field as the reactive A particles enter the field. The resulting carbonic acid particles, in accordance with the reaction equation (3), will be swept downstream by the advective flow to cause precipitation reaction uniformly along the direction transverse to flow at some distance downstream. This pattern of alternating dissolution and precipitation areas at identical intervals in the downstream direction will repeat itself, the resulting pattern being reminiscent of a precipitation banding phenomenon [Singurindy and Berkowitz (2003)]. Again, in this case no heterogeneity in the direction transverse to flow is expected to emerge, thus we suggest that no transport self-organization will occur as well.

Following the above discussion, we argue that for the transport self-organization to emerge in an initially homogeneous field undergoing a dissolution/precipitation reactive process as defined in our reactive setup, it is necessary for the transport mechanism to include both diffusive and advective contributions. Here, the stochastic diffusion leads to local concentration variations in H^+, that in turn create local variations in hydraulic conductivity, while the advection follows these conductivity variations, funneling the flow towards the higher conductivity areas and further increasing their conductivity due to the enhanced dissolution by the funneled A particles. This creates positive coupling between the reactive and transport processes. Here, an analogy can be made to the Turing's morphogenesis model (see Section 1.2), where the homogenizing action of the diffusion is counteracted by the fact that the diffusion coefficients of the reacting substances differ, which is a prerequisite for the appearance of self-organizing patterns. We suggest that the driving force for transport self-organization in the model under investigation is the ratio between the diffusive to advective transport rates, or the reciprocal of the Peclet number. Therefore, we expect to obtain an increase in transport self-organization in the field with a decrease in the Peclet number of the flow.

3.2 Self-organization quantization employing Shannon entropy

Having obtained a qualitative understanding of the subject of self-organization in the context of reactive transport of the porous medium, we shall now seek for a way to characterize this phenomenon quantitatively using a concept of Shannon entropy, also referred to as "information entropy". Shannon entropy was introduced originally in the field of communication theory, whose fundamental problem is formulated as "*reproducing at one point either exactly or approximately a message, selected at another point.*" [Shannon (1948)]. Viewing communication as a statistical process, Shannon employed an entropy-like parameter to provide a measure for the amount of transmitted information, carried by a certain sequence of symbols (a message). Appendix B contains a short account of the Shannon entropy, while here we only reprint the main result

$$S = -\Sigma_i \, p_i \log_2 p_i \tag{12}$$

https://doi.org/10.5194/hess-2023-84
Preprint. Discussion started: 8 May 2023


Hydrology and Earth System Sciences
Discussions

where S is the Shannon entropy per symbol of the message and $p_i = n_i/n,\ i = 1...N_s$ are the relative occurrence frequencies of N_s different symbols that constitute the message, calculated as a ratio of the number of occurrences of a specific symbol i in the message n_i to the total message length n.

The definition of information entropy, given by Shannon, is equivalent to physical entropy in statistical mechanics as defined by Gibbs, where the logarithm in (12) is to the base of e and the sum is multiplied by the Boltzmann constant [Ben-Naim (2008)]. The statistical definition of a physical entropy characterizes the number of possible microstates of a system that are consistent with its macroscopic thermodynamic properties which constitute the macrostate of the system. Thus, in case of a gas consisting of a large number of molecules in a container, a microstate of the system consists of position and momentum of each molecule, as it moves within the container, colliding with other molecules and container walls. A multitude of such microstates correspond to a single macroscopic state of the system, defined by its pressure and temperature. The parameter p_i in this case corresponds to a probability that a microstate i occurs during the system's fluctuations. According to the second law of Thermodynamics, entropy of a system reaches its maximum value at equilibrium, where gradients of thermodynamic parameters are depleted by dissipative forces and the measure of order in the system is at its minimum. In this case, each microstate is equally likely and p_i is simply the inverse of the total number of microstates (Kondepudi and Prigogine, 1998).

To characterize the emergence and development of transport self-organization in an initially homogeneous field as the dissolution-precipitation reactive processes in the field evolve, we adopt a straightforward use of the Shannon entropy, in a similar vein to Zehe et al. (2021), where it was employed in the context of characterizing self-organization in heterogeneous non-reactive groundwater systems. In order to place all results on equal footing, we perform additional computational *non-reactive* tracer tests on the snapshots of the hydraulic conductivity field at different simulation times, as suggested in Section 3.1. The non-reactive particle tracer algorithm, employed for this purpose, consists of the flow and particle transport algorithm as described in Section 2.2, but without the kinetic reaction part. A total number of $N_{tot}^{NR} = 1e5$ particles, that represent the non-reactive tracer solute (not to confuse with the number of reactive particles N_{tot} injected per T_{pv} in the reactive algorithm), are injected at the inlet of the computational field, subject to identical hydraulic pressure head drop boundary condition of $\Delta h = 100cm$, and allowed to advance within the field subject to laws described in Section 2.2, until all of them reach the outlet boundary. The relatively large value of Δh is chosen in order to eliminate the diffusive transport contribution which tends to smooth out concentration gradients due to its stochastic character. The injected particles are flux-weighted according to the conductivity distribution of the inlet cells. The field density matrix, obtained by counting the total number of particle visitations in each computational cell, is recorded for each field snapshot. From this matrix, the solute concentration distribution of the non-reactive tracer across the field is obtained. We recall the proposition put forth by Berkowitz and Zehe (2020) that solute transport self-organization corresponds to an emergence of solute transport gradients in the field in the direction transverse to the direction of the flow. To quantify the entropy of transport self-organization in the snapshots of the hydraulic conductivity field, we rewrite (12) as follows

$$S(x) = -\Sigma_i p_i \log_2 p_i \tag{13}$$

https://doi.org/10.5194/hess-2023-84
Preprint. Discussion started: 8 May 2023


Hydrology and Earth System Sciences
Discussions

where $S(x)$ is the Shannon entropy of the transversal solute concentration at a given axial coordinate x and $p_i = N_i/N_{tot}^{NR}$, $i = 1...N_y$ is the relative solute concentration distribution at x in the direction transverse to flow (here, N_i is the number of particles that have passed through the i-th cell at x).

3.3 The relation between self-organization and hydraulic power

Following the thermodynamic framework, as applied to the system under investigation, energy must be invested in the heterogeneous field to maintain an ordered state of solute transport there. This energy comes in the form of hydraulic power that enables the flow to overcome the hydraulic resistance of the porous medium under the applied hydraulic pressure head drop boundary condition. Following the reasoning of Zehe et al. (2021) that the measure of transport self-organization is directly related to the degree of heterogeneity of the porous medium, we consider the following simple 1D example of a fluid flowing through a series of N porous medium cells in an attempt to better understand the relation between the degree of heterogeneity of the porous medium and the hydraulic power required for the fluid to overcome the resistance of the medium under the inlet-outlet hydraulic head drop boundary condition. Given that the hydraulic conductivity of the i-th cell is k_i, the total hydraulic power invested by the fluid to overcome the hydraulic resistance of the cells is given by

$$P = \rho g \Sigma_{i=1}^{N} \nabla h_i \cdot q_i \tag{14}$$

where ∇h_i and q_i are the hydraulic head gradient and Darcy flux through the i-th cell, ρ is the fluid density and g is the gravitational acceleration. Using Darcy's law and recognizing that the Darcy flux is constant through the cells, we get

$$P = -\rho g q^2 \Sigma_{i=1}^{N} 1/k_i \tag{15}$$

Thus, hydraulic power in a 1D series of cells depends on the expression $\Sigma_{i=1}^{N} 1/k_i$. Going back to the system under investigation and assuming that the degree of heterogeneity in the field, that emerges due to the reactive process, is minor, so that the streamlines in the field remain mostly horizontal, this result can be applied to our 2D computational field. In the beginning of the simulation the field is completely homogeneous, therefore all k_i are equal. However, with time, as the coupling between the reactive and transport processes intensifies the heterogeneity of the field, the scatter of k_i increases. Assuming that the changes in the mean value of the k_i distribution are minor, the expression $\Sigma_{i=1}^{N} 1/k_i$ obtains its minimum for the completely homogeneous case and grows with the increase in the scatter of k_i. Assuming also that the changes in the Darcy flux q with time are minor, we conclude that an increase in heterogeneity of an initially homogeneous porous medium due to the coupled reactive process requires an increase in the hydraulic power, supplied to the flow to overcome the hydraulic resistance of the medium under the maintained hydraulic head drop boundary condition, applied to the field. Within the adopted thermodynamic framework, this increase in power allows to increase the spatial self-organization of the solute transport in the medium.

4 Results and discussion

Based on the reactive transport algorithm described in Section 2, we demonstrate the emergence and evolution of transport self-organization in an initially homogeneous porous medium along with the advancement of the reactive process, and showcase that

https://doi.org/10.5194/hess-2023-84
Preprint. Discussion started: 8 May 2023


Hydrology and Earth System Sciences
Discussions

transport self-organization correlates with the Peclet number of the flow. To investigate this relation, we simulate a number of reactive transport scenarios for different values of the ratio of advective to diffusive transport rates, characterized by the Peclet number, calculated as shown in Section 2.4. This is achieved by applying different values of the inlet-outlet hydraulic pressure head boundary condition Δh, as described therein. Thus, for Δh = 1e-4, 1e-3, 1e-2 and 1e-1 [cm], we obtain the transport Peclet number to be approximately Pe= 0.38, 1.2, 3.8 and 12.0. A reaction enhancement by a factor of 5e2 is employed (see Section 2.3). We follow this series of analyses by quantifying the evolution of transport self organization in time, showing that a decrease in the Peclet number leads to an increase in transport self-organization in the field, as expressed by a decrease in the Shannon entropy. The self-organization of the breakthrough curve exhibits the opposite tendencies, that are explained from the thermodynamic perspective. The hydraulic power, required to maintain the driving head pressure drop boundary condition between inlet and outlet, increases with the increasing variance of the hydraulic conductivity in the field due to the evolution of the reactive process in the field. This increase in power results in an increase in the transport self-organization in the field.

4.1 Evolution of reactive process in the field

We begin by examining the evolution of the reactive process, as depicted by the snapshots of the relative hydraulic conductivity $K - K_0$ of the field at different normalized times $\tilde{t} = t/T_{pv}$, shown in Figures 1a–c (obtained from a realization of the reactive process for $Pe = 0.38$). As the reactive particles advance and react in the initially homogeneous field, heterogeneity is being introduced into the field in the form of local dissolution and precipitation areas, signified by positive and negative values of $K - K_0$, respectively. This heterogeneity advances downstream alongside the reactive particles, with the local dissolution / precipitation areas intensifying with time as the reactive process in the field develops, creating a clearly distinguishable reaction front. Downstream of the front, the field remains homogeneous as the reactive process hasn't arrived there yet. A dissolution area is located In the immediate vicinity of the inlet, where the chemical equilibrium is tilted towards dissolution; this correlates with experimental and simulation observations [Poonoosamy et al. (2020), Deng et al. (2022)]. Figure 1d presents the overall disposition of dissolution (cyan) and precipitation (blue) areas as the pore volume time is reached ($\tilde{t} = 1$). Note that the dissolved areas are well connected, while the precipitated areas are isolated. The correlation length of these fields was found to be of the order of the size of the computational cell, therefore no larger structures in the conductivity distribution are observed.

The influence of the Peclet number on the evolution of reactive process in the field is characterized in Figures 2a–d. Figure 2a presents the global reaction rate $\dot{R}$, which was calculated as the mean value of the absolute rate of change of hydraulic conductivity with dimensionless time $|dk/d\tilde{t}|$ over all computational cells, as a function of dimensionless time $\tilde{t}$. This parameter takes into an account the overall amount of reaction that takes place, including both dissolution and precipitation. The calculation was performed excluding the area of 10 computational cells in the immediate vicinity of the inlet, so to focus on the evolution of the reactive process within the field, excluding the inlet conductivity alteration; this is ignored since this effect is of a very localized nature. We observe that the reaction increases with dimensionless time in a linear fashion, as the reactive particles sample more of the field's territory at an approximately constant mean velocity, which allows broader opportunities

https://doi.org/10.5194/hess-2023-84
Preprint. Discussion started: 8 May 2023

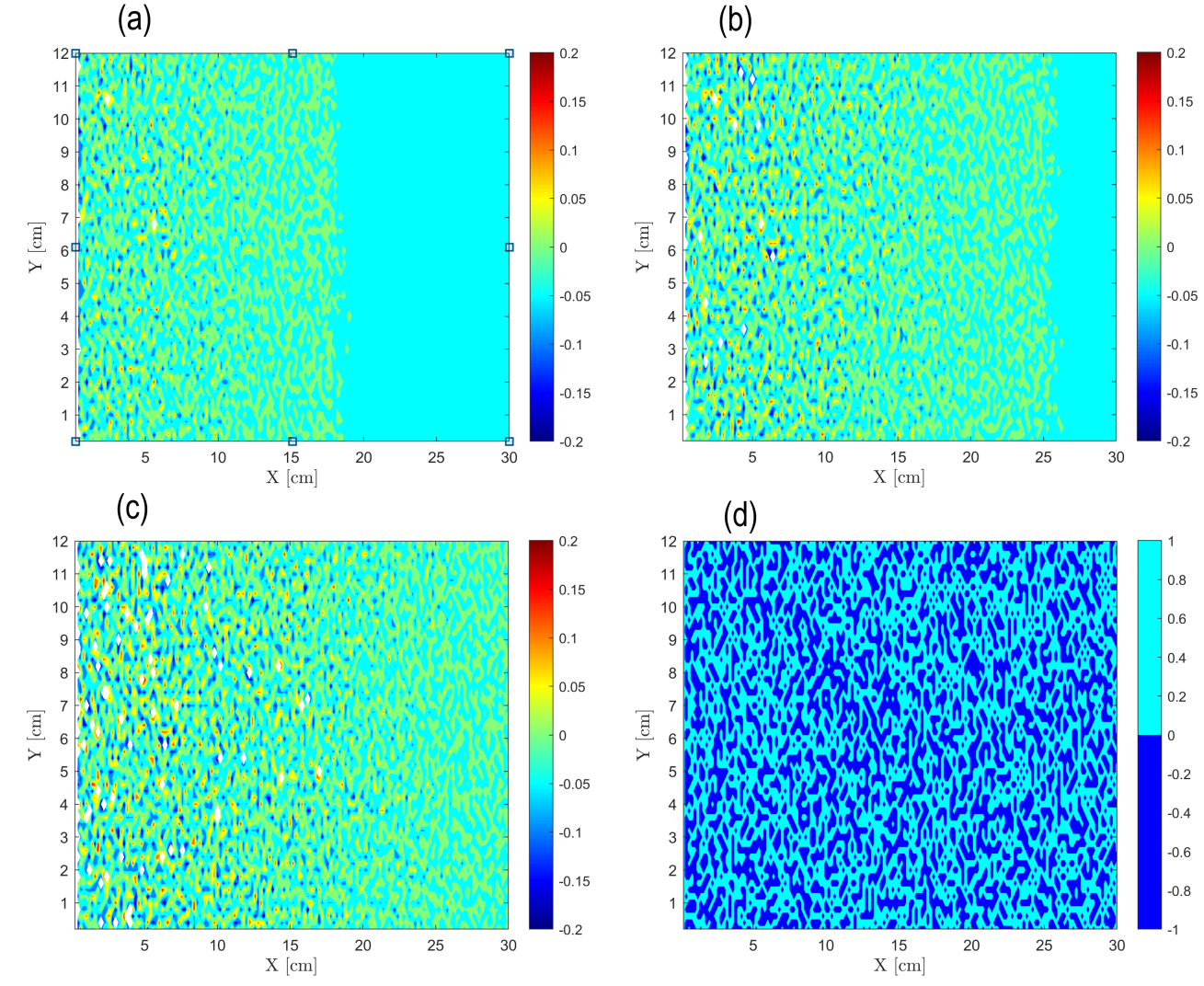

Figure 1. Evolution of the relative hydraulic conductivity $K - K_0$ field over time for Pe = 0.38: (a) $\tilde{t} = 0.5$, (b) $\tilde{t} = 0.72$, (c) $\tilde{t} = 0.94$. Panel (d) shows overall disposition of dissolution (cyan) and precipitation (blue) areas at $\tilde{t} = 0.94$.

https://doi.org/10.5194/hess-2023-84
Preprint. Discussion started: 8 May 2023


Hydrology and Earth System Sciences
Discussions

for reaction. Beginning from $\tilde{t} = 1$, $\dot{R}$ becomes approximately constant, as the reactive particles have sampled an entire field at that point. The influence of the Peclet number is clearly exhibited by the fact that the global reaction rate increases with the reciprocal of Peclet, showing that diffusive transport mechanism, responsible for mixing in the field, enhances the reactive process. This can be explained by the fact that diffusion, being stochastic in nature, allows particles to sample regions also in the transverse direction, away from the path suggested by the advection mechanism, which allows a better chance for reaction. This result further confirms the findings of [Nissan and Berkowitz (2019)] on bimolecular reaction, where an increase in the reactant production rate with a decrease in Peclet was reported, due to an increase in the spatial spread of the transported species; this trend was also reported in Edery et al. (2021). An interesting property of the reaction rate is its scalability with the Peclet number. Assuming separation of variables in $\dot{R}$, so that $\dot{R} = f(\tilde{t}) \cdot g(Pe)$ and the Peclet dependency takes on the power law form $g(Pe) = a \cdot Pe^b + c$, satisfying results were obtained for $a, b, c = 3.0, -1.0, 4.1$ ($R^2 = 0.982$). The scaled curves, obtained by dividing the computed curves by the estimated $g(Pe)$, are depicted in the figure inset. Thus, the dependence of the global reaction rate $\dot{R}$ on the Peclet number is in the form of the reciprocal of Peclet.

Figure 2b presents the normalized global reaction rate $\dot{R}_{norm}$, that was obtained by normalizing the global reaction rate $\dot{R}$ by the distance from outlet sampled by the flow $L\tilde{t}$ (excluding the area in the vicinity of the inlet). This was done in order to obtain an indication of the reaction rate per unit area where the reaction takes place. After the transitional effects fade, $\dot{R}_{norm}$ exhibits an approximately constant behavior, as expected. Recall that on a local scale in our model the reaction is instantaneous [Edery et al. (2021)]. Here, as well, the scalability with the Peclet number exists, taking the same form as in the case of the non-normalized global reaction rate $\dot{R}$. The scaled curves are depicted in the figure inset. Again, the dependence on the Peclet number is in the form of the reciprocal of Peclet.

Figure 2c presents the deviation of the mean value of hydraulic conductivity over all computational cells from the initial conductivity $\tilde{K} - K_0$ as a function of dimensionless time $\tilde{t}$. Here, the area of 10 computational cells in the immediate vicinity of the inlet was excluded from the calculation as well. Clearly, the net reaction is tilted towards dissolution, as $\tilde{K} - K_0$ grows monotonously with $\tilde{t}$, which is reasonable due to the influx of low pH fluid at the inlet of the field (see also Edery et al. (2021)); the relative increase in hydraulic conductivity is small comparing to K_0. This result is in agreement with the findings of Edery et al. (2021). The power law shape holds well, beginning with approximately $\tilde{t} = 0.3$. The onset of the power law region coincides with the time when a large enough number of particles has reacted within the field to create a statistically consistent picture. The curves for larger Peclet numbers exhibit fluctuations for the considerable portion of time, however they comply with the power law shape eventually as well. $\tilde{K} - K_0$ also increases with the decrease of the Peclet number, again due to the reaction enhancing role of the diffusive transport mechanism. Here, as well, the scalability with the Peclet number exists. Assuming again separation of variables as before, so that the Peclet dependency takes on the power law form $g(Pe) = a \cdot Pe^b + c$, good results were obtained for $a, b, c = 0.007332, -1.0, 0.0$ ($R^2 = 0.982$). Again, the dependence of $\tilde{K} - K_0$ on the Peclet number is in the form of the reciprocal of Peclet. The scaled curves are depicted in the figure inset.

https://doi.org/10.5194/hess-2023-84
Preprint. Discussion started: 8 May 2023

Hydrology and Earth System Sciences
Discussions
Open Access
EGU

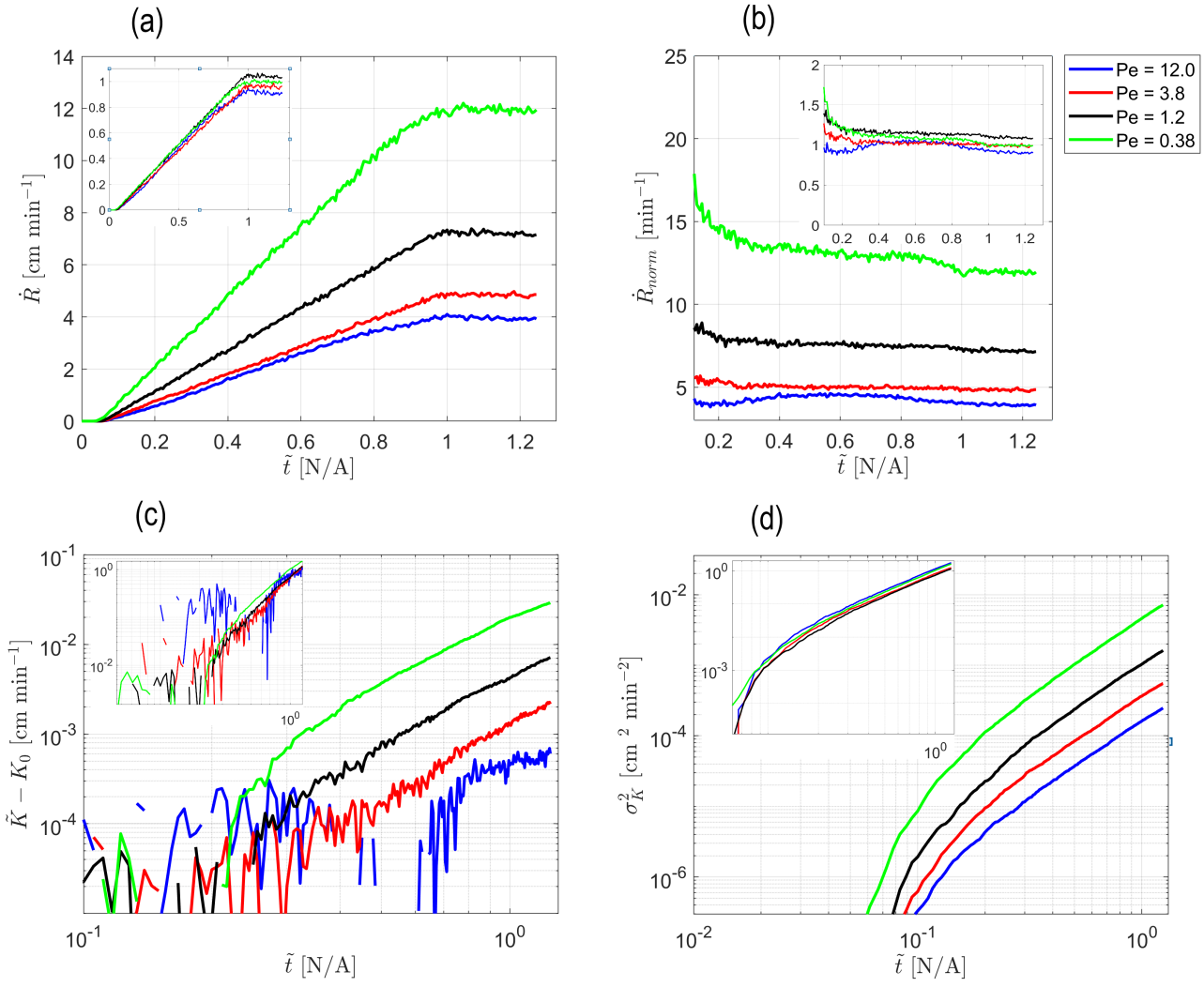

Figure 2. influence of Peclet number on the evolution of the reactive process in the field over time: (a) Global reaction rate $\dot{R}$, (b) Normalized global reaction rate $\dot{R}_{norm}$, (c) Deviation of the mean hydraulic conductivity from initial value $\tilde{K} - K_0$ and (d) Hydraulic conductivity variance σ^2_k, as a function of dimensionless time $\tilde{t}$. Insets show Peclet-scaled curves, obtained by assuming a power-law Peclet dependency (a dependency on the reciprocal of Peclet was obtained for all displayed parameters, as an exponent value of -1 resulted in a satisfying fit for all curves).

https://doi.org/10.5194/hess-2023-84
Preprint. Discussion started: 8 May 2023


Hydrology and Earth System Sciences
Discussions

Similar trends are observed in Figure 2d, that presents the variance of hydraulic conductivity σ_k^2 as a function of dimensionless time $\tilde{t}$. Here, the area of 10 computational cells in the immediate vicinity of the inlet was excluded from the calculation as well. This parameter, being the measure of the field's heterogeneity, is indicated as the primary cause for transport self-organization in the field [Zehe et al. (2021)]. σ_k^2 increases monotonously with dimensionless time $\tilde{t}$, as the particles sample more field regions and react at an increasing rate, this result again being in agreement with the findings of Edery et al. (2021). Heterogeneity also increases with the decrease of the Peclet number, again due to the reaction enhancing role of the diffusive transport mechanism. We thus state that reactive transport scenarios with low values of Peclet number, corresponding to dominant diffusive transport mechanism, coincide with an increased reaction rate in the field and, thus, increased field's heterogeneity. The power law shape holds well for all Peclet cases, beginning with approximately $\tilde{t} = 0.2$. Turning again to the findings of Edery et al. (2021), where the coupled reactive process was investigated within the framework of the continuous time random walk (CTRW) approach, we emphasize the anomalous (non-Fickian) nature of the ensuing transport, that is traced back to the coupling between the reactive and transport processes in the initially homogeneous field. Here, as well, the scalability with the Peclet number exists. Assuming again separation of variables as before, so that the Peclet dependency takes on the power law form $g(Pe) = a \cdot Pe^b + c$, good results were obtained for $a, b, c = 0.001692, -1.0, 0.0$ ($R^2 = 0.987$). Again, the dependence of σ_K^2 on the Peclet number is in the form of the reciprocal of Peclet. The scaled curves are depicted in the figure inset. The dependence of the parameters, depicted in Figures 2a–d, on the reciprocal of the Peclet number confirms that this dimensionless number is indeed the driving force behind the evolution of the reactive process in the porous medium.

It is also of interest to consider the limiting cases of the model under investigation, as suggested in Section 3.1. For high Peclet numbers, the transport in the field is advection-dominated and the diffusive mixing effects are insignificant, therefore the difference between the neighboring curves in Figure 2 decreases significantly in this region. For the lower Peclet curves, corresponding to diffusion-dominated flow, the difference between curves is clearly distinguished and is growing with the further decrease in Peclet. An important note should be made regarding the initial state of the field that undergoes reactive process: in our case of an initially homogeneous field, diffusion acts as an enhancing factor for the emergence of heterogeneity in the field; in an initially heterogeneous case, such as in [Al-Khulaifi et al. (2017)], diffusion is capable of decreasing the heterogeneity of the porous medium due to its smoothing property.

4.2 Transport self-organization in the field

To characterize the emergence and development of transport self-organization in our model as the dissolution-precipitation reactive processes in the field advance, we adopt a straightforward use of the Shannon entropy, similar to Zehe et al. (2021), where it was employed in the context of characterizing self-organization in non-reactive flows in heterogeneous groundwater systems. In order to place all results on equal footing, we perform computational *non-reactive* tracer tests on the snapshots of the hydraulic conductivity field at different values of the dimensionless time $\tilde{t}$, as described in Section 3.2.

The emergence of transport self-organization in the reacting field is evident from the Figures 3a-d that present the decimal

https://doi.org/10.5194/hess-2023-84
Preprint. Discussion started: 8 May 2023


Hydrology and Earth System Sciences
Discussions

logarithm of the relative non-reactive tracer concentration $c - \tilde{c}$, defined as the deviation of the non-reactive particle visitations from the equilibrium state (represented by perfect mixing in the field), in the snapshots of the field that undergoes reactive process at $Pe = 0.38$, for different values of the dimensionless time $\tilde{t}$. Here, c is the number of non-reactive particles that have visited a specific cell (local concentration) and $\tilde{c} = N_{tot}^{NR}/Ny$ is the mean concentration value obtained in the case of a completely homogeneous field. This parameter is analogous to the non-reactive solute relative concentration obtained from the tracer tests. With the passage of time, variations in the hydraulic conductivity of the field due to the reactive process create autocatalytic feedback mechanism that leads to an emergence of finger-like preferential flow paths. These paths interact, competing for the available flow, so that eventually some of the paths carry a significantly larger part of the injected particles than the others, as seen from the increasing concentration gradients in the direction transverse to flow. The overall straight linear shape of the paths is explained by the relative smallness of the conductivity variations, produced by the reactive process. Another reason for this is that the correlation length of the produced heterogeneous fields is small as well, leading to absence of large-scale structures, that could alter significantly the direction of the preferential flow paths. The simulated scenario is similar to that of reactive infiltration, reported in Szymczak and Ladd (2006), where a pore-scale numerical model was used to investigate channel growth and interaction due to dissolution in fractures. Their model employed Lattice-Boltzmann method for flow field calculation, while the transport of dissolved species was modeled by a random walk algorithm that efficiently incorporates the chemical kinetics at the solid surfaces. They reported the emergence of a solid-fluid interface instability, with undulation areas formed first at the solid-fluid interface of the porous media due to dissolution, which are later transformed into well-defined finger-like channels or wormholes, that rapidly advance into the medium; as dissolution proceeds, these fingers interact, competing for the available flow, and eventually the growth of the shorter ones ceases.

The observations from Figure 3 are confirmed by the plot of the normalized Shannon entropy of the transport in the field $S_{norm} = (S - S_{max})/S_{max}$ vs. normalized distance from inlet $\tilde{x} = x/L$, calculated from the non-reactive solute concentration data in the snapshots of reactive field at different values of dimensionless time $\tilde{t}$ for $Pe = 0.38$, presented in Figure 4a. Here, S is the Shannon entropy of the transport in the field as a function of the distance from inlet X, calculated from (13) and S_{max} is the maximal possible transport entropy value in the field, calculated as discussed in Section 3.2, so that S_{norm} obtains values from 0 (maximum entropy, no self-organization) to -1 (minimum entropy, maximum self-organization, corresponding to a single preferential flow path channeling all injected solute particles). As the reactive process in the field advances, the resulting level of transport self-organization in the field increases as it reaches further downstream alongside the reaction front, which is signified by the decrease in S_{norm}. Figure 4b presents the mean value of the normalized Shannon entropy of the transport in the field, averaged over the field, $\tilde{S}_{norm}$, vs. dimensionless time $\tilde{t}$ for different values of Peclet number. Again, the plot clearly shows an increase in the transport self-organization in the field with the advance of the reactive process, as the mean normalized entropy $\tilde{S}_{norm}$ decreases over time. A clear picture emerges, where the level of self-organization directly correlates with the Peclet number of the reactive flow, as the normalized entropy $\tilde{S}_{norm}$ decreases with decrease in Peclet. This clearly signifies that diffusive transport mechanism is dominant in initiating transport self-organization in an initially homogeneous field via the coupled reactive process, as it is manifested most significantly for low Peclet numbers that correspond to

https://doi.org/10.5194/hess-2023-84
Preprint. Discussion started: 8 May 2023

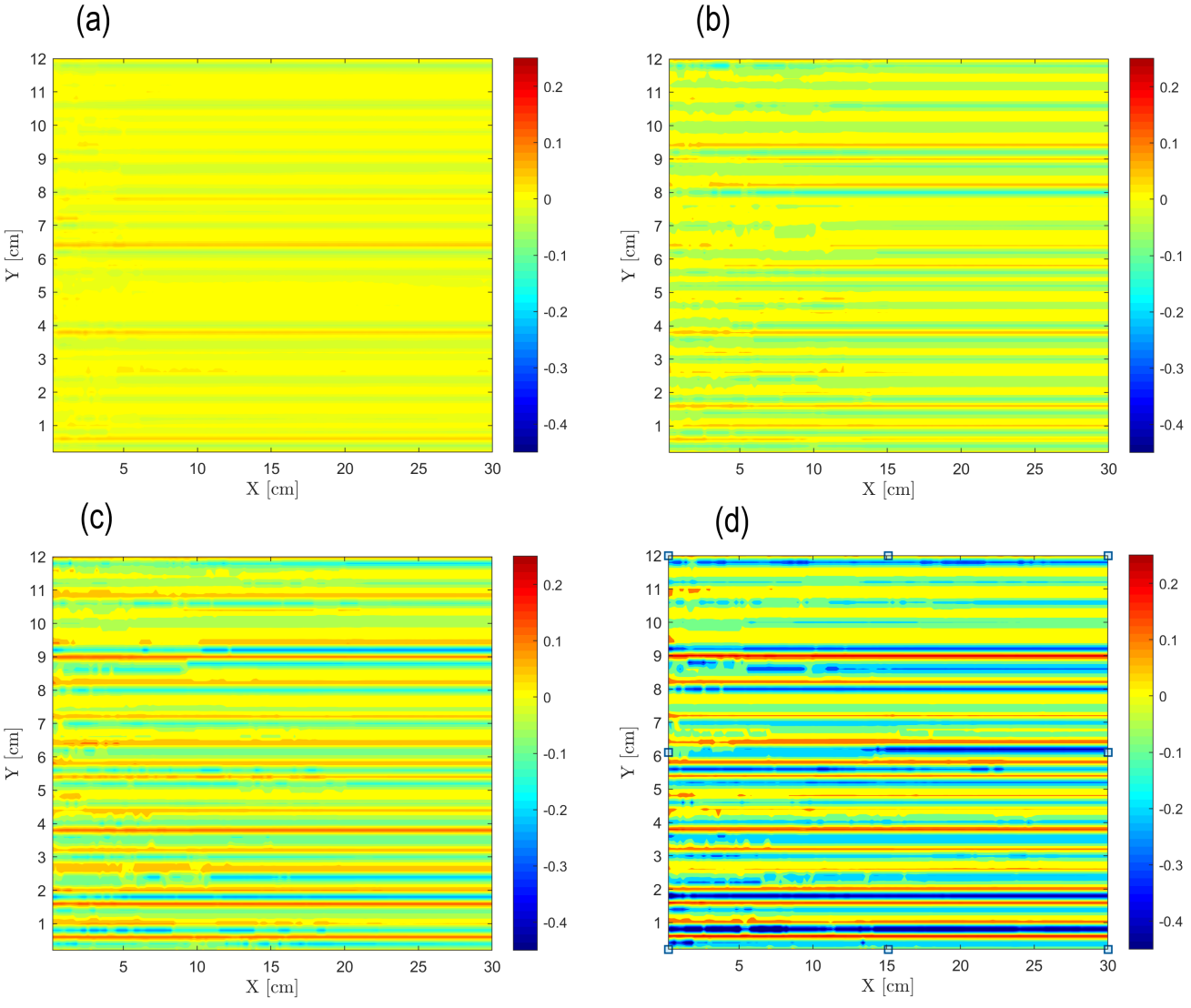

Figure 3. Evolution of the transport self-organization in the field for Pe = 0.38, as represented by the relative non-reactive tracer concentration $c - \tilde{c}$, based on data obtained from the non-reactive tracer tests peformed on the snapshots of the field over time (a single realization of the reactive process): (a) $\tilde{t} = 0.24$, (b) $\tilde{t} = 0.51$, (c) $\tilde{t} = 0.76$ and (d) $\tilde{t} = 0.96$.

https://doi.org/10.5194/hess-2023-84
Preprint. Discussion started: 8 May 2023

diffusion-dominated flow. For lower values of Peclet number, the difference between the neighboring curves is clearly distinguished, while for larger Peclet numbers, where advection becomes dominant, this difference diminishes, further supporting our discussion on limiting cases for the model under investigation, as discussed in Section 3.1.

In this context, it is interesting to consider the findings of Zehe et al. (2021) that showed a clear correlation between the field's heterogeneity measure (statistical variance of the field's conductivity) and the self-organization of the field's transport, as represented by the Shannon entropy of the solute concentration matrix, in non-reactive transport in heterogeneous fields. Their results showed a clear decrease in Shannon entropy following an increase in the field's heterogeneity. These results are given further confirmation in our study, as, with the passage of time, the development of the reactive process in an initially homogeneous field results in an increase of its heterogeneity (Figure 2b), accompanied by a decrease in the Shannon entropy of the transport in the field that corresponds to an increase in transport self-organization (Figure 3). To conclude our findings thus far, we state that the reactive transport at lower Pe numbers, corresponding to diffusion-dominated flow, results in a higher field heterogeneity and, thus, stronger transport self-organization in the field. An important note should be made regarding the initial state of the field that undergoes reactive process: in our case of an initially homogeneous field, diffusion acts as self-organization enhancer; in an initially heterogeneous case, diffusion is capable of decreasing the transport self-organization due to its smoothing property.

The Peclet number scalability is also exhibited in the Shannon entropy of transport self-organization. Assuming again separation of variables in $\tilde{S}_{norm}$, so that $\tilde{S}_{norm} = f(\tilde{t}) \cdot g(Pe)$ and the Peclet dependency takes on the power law form $g(Pe) = a \cdot 2^{b \cdot Pe} + c$, satisfying results were obtained for $a, b, c = -0.02665, -1.0, -0.000273$ ($R^2 = 0.9942$). Thus, the mean normalized Shannon entropy of transport self-organization depends on the reciprocal of 2 to the power of Peclet number. The origin of this relation can be traced back to the Shannon entropy formula (13), where a logarithm to the base of 2 appears. The free coefficient c is expected to be zero, since in the high-Peclet limit we expect to obtain no transport self-organization in the field; deviation from this value is attributed to statistical errors that can be decreased by averaging results from several realizations of the reactive process. The scaled curves are depicted in the figure inset. This dependence of the mean normalized Shannon entropy of transport self-organization on the Peclet number confirms that this dimensionless number is indeed the driving force behind the transport self-organization in an initially homogeneous porous medium.

4.3 Entropy export into the break through curve

As a next stage in the analysis of transport self-organization in the reactive field, we turn to the particle breakthrough curve in an attempt to analyze the influence of self-organization of the field's transport on the particle arrival times. Figure 5a shows the temporal breakthrough curves calculated from the non-reactive particle tracking tests performed on the snapshots of the reacting field for $Pe = 0.38$, as described in Section 3.2. The width of support of the breakthrough curves clearly increases with time, indicating an increasing scatter in non-reactive particles arrival times as the field's heterogeneity grows larger. Especially, a significant increase in the tailing arrival times is observed.

https://doi.org/10.5194/hess-2023-84
Preprint. Discussion started: 8 May 2023

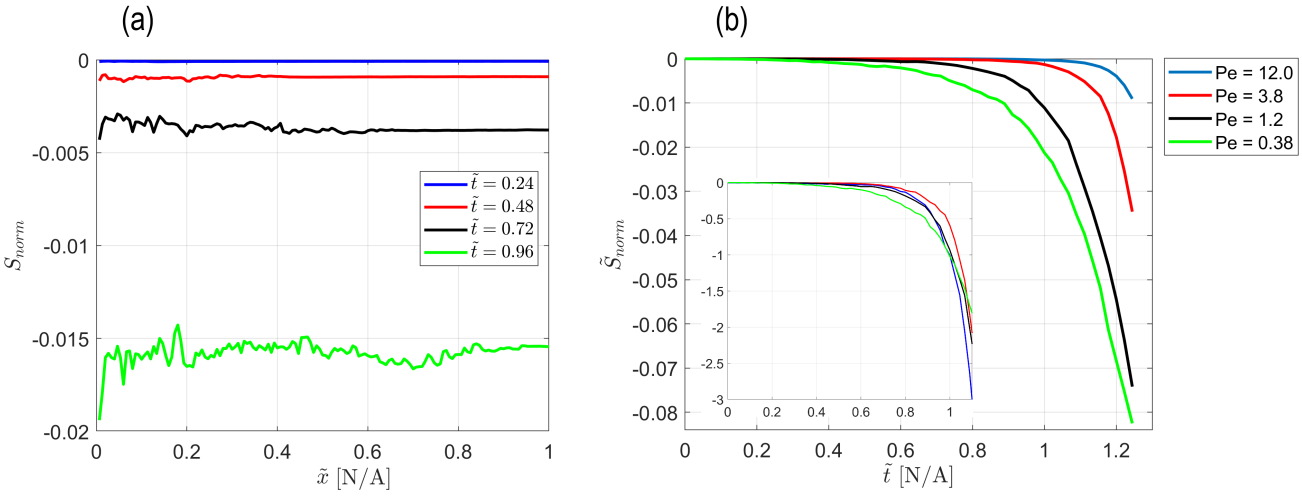

Figure 4. Self-organization of the transport in the field via normalized Shannon entropy $S_{norm} = (S - S_{max}/S_{max})$: (a) S_{norm} vs. normalized distance from inlet $\tilde{x} = x/L$ at different dimensionless times $\tilde{t}$ for $Pe = 0.38$, (b) Mean value of the normalized entropy over the field $\tilde{S}_{norm}$ vs. dimensionless time $\tilde{t}$ for different values of Pe. Inset shows Peclet-scaled curves, obtained by assuming a power-law Peclet dependency.

The Shannon entropy of the breakthrough curves was calculated by dividing the arrival times span into 5000 bins and employing equation (13) with p_i as the relative occurrences of arrival times. To place all results on equal footing, the arrival time span was taken identical for all Peclet values. Figure 5b presents the normalized breakthrough curve entropy, calculated as $S^{BTC}_{norm} = (S^{BTC} - S_{max})/S_{max}$, vs. dimensionless time $\tilde{t}$. Here, S^{BTC} is the breakthrough curve entropy, calculated from (13) and S_{max} is the maximal possible entropy value, obtained in the case of a perfectly uniform distribution of arrival times (similarly to the discussion of S_{max} estimation for the field transport entropy held in Section 3.2, in the case of division of the arrival times span into 5000 bins, this value will be $\log_2 5000$). Again, S^{BTC}_{norm} obtains values from 0 (no self-organization) to -1 (maximum self-organization, corresponding to the case when all particles arrive at the outlet at the same time).

A picture emerges, where the Shannon entropy of the arrival times increases with the passage of time, reflecting a larger uncertainty and a declining order in the temporal distribution of travel times. This corresponds to an increase in both the field's heterogeneity and the self-organization of transport, as the reactive process in the field evolves. We also observe that the level of self-organization in arrival times directly correlates with the Peclet number, as the normalized breakthrough entropy S^{BTC}_{norm} decreases with increase in Peclet, an opposite tendency comparing to the entropy of the field transport.

https://doi.org/10.5194/hess-2023-84
Preprint. Discussion started: 8 May 2023

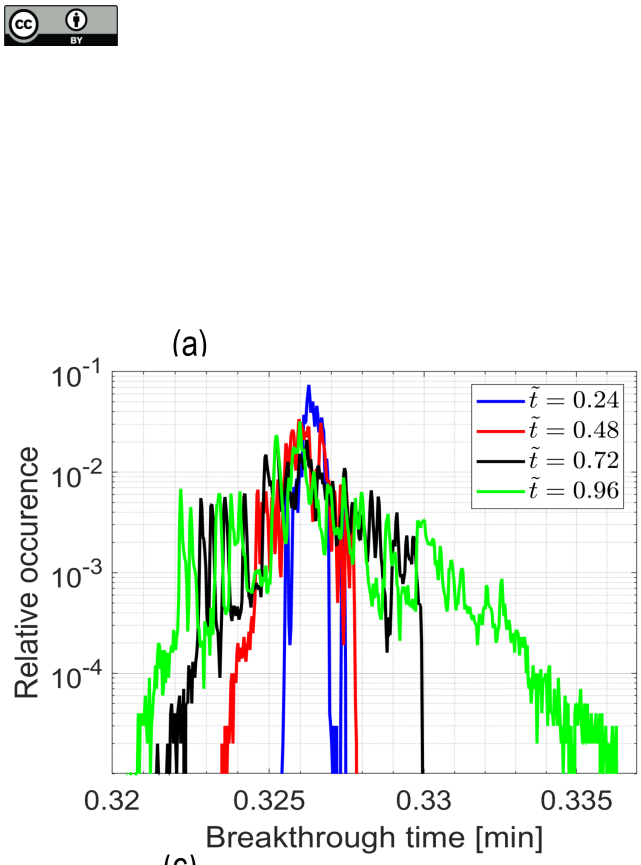

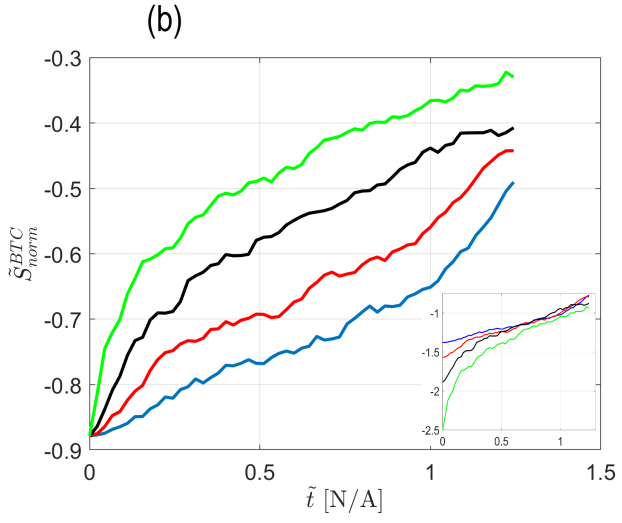

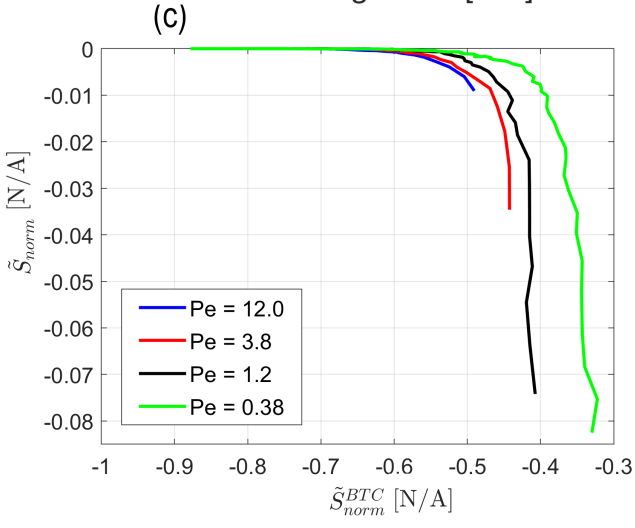

Figure 5. Breakthrough curve self-organization: (a) Histogram of the non-reactive particle arrival times in snapshots of the reacting field at different dimensionless times $\tilde{t}$ for $Pe = 0.38$, (b) Normalized breakthrough curve entropy $\tilde{S}^{BTC}_{norm}$ vs. dimensionless time $\tilde{t}$ for different values of Peclet number (the inset shows Peclet-scaled curves) and (c) Normalized field transport entropy $\tilde{S}_{norm}$ vs. Normalized breakthrough curve entropy $\tilde{S}^{BTC}_{norm}$ for different values of Peclet number.

https://doi.org/10.5194/hess-2023-84
Preprint. Discussion started: 8 May 2023


Hydrology and Earth System Sciences
Discussions

The Peclet number scalability is also exhibited in the Shannon entropy of the breakthrough curve, from approximately $\tilde{t} = 0.5$. Assuming again separation of variables in $\tilde{S}^{BTC}_{norm}$, so that $\tilde{S}^{BTC}_{norm} = f(\tilde{t}) \cdot g(Pe)$ and the Peclet dependency takes on the power law form $g(Pe) = a \cdot Pe^b + c$, satisfying results were obtained for $a, b, c = 0.5511, -0.1686, -1.0$ ($R^2 = 0.9762$). The free coefficient c obtains the value of -1, because in the high-Peclet limit we expect to obtain maximal self-organization in the breakthrough times.

The tendencies presented in Figure 5b are further supported by Figure 5c that shows the normalized field transport entropy $\tilde{S}_{norm}$ as a function of the normalized breakthrough curve entropy $\tilde{S}^{BTC}_{norm}$ for different values of Peclet number: $\tilde{S}_{norm}$ decreases monotonously with an increase in $\tilde{S}^{BTC}_{norm}$ for all values of Peclet number. These results can be explained straight-ahead in terms of the degree of the field's heterogeneity: for lower Peclet values, the reactive transport in the field leads to a higher degree of heterogeneity, which is responsible for a greater scattering in arrival times due to the variety of paths particles may take on their way to outlet; this is reflected in the overall smoothing out of the breakthrough curve and, as a result, in the breakthrough curve entropy that grows with the degree of scattering in arrival times. An alternative observing perspective on the arrival times can be formulated in thermodynamic terms [Zehe et al. (2021)]: since the transport entropy within the field is decreasing for lower Peclet values and, according to the second law of Thermodynamics, the overall entropy of the system and its surroundings cannot decrease, the entropy, produced within the field needs to be exported outside (see Appendix A); this is reflected in the increased entropy of the breakthrough curve. This statement should be regarded on a qualitative level only, as, due to different spatial and temporal discretizations, changes in the Shannon entropies of the field transport and the breakthrough curves with the passage of time do not comply.

4.4 Hydraulic power - entropy relation

The evolution of the reactive process in an initially homogeneous field is accompanied by the emergence of heterogeneity and, consequently, transport self-organization in the field. This demands that an increased energy is supplied to the field to maintain an increasingly ordered state that emerges there. This energy is supplied in the form of hydraulic power, required for the flow to overcome the hydraulic resistance of the porous medium. In our model, the hydraulic power is supplied due to the inlet-outlet hydraulic head drop boundary condition applied to the porous medium, that works similarly to a pump. Figure 6a presents the net hydraulic power in the field $P - P_0$ as a function of $\tilde{t}$ for different Peclet numbers. Here P is calculated according to (14) and P_0 is the initial power that corresponds to a completely homogeneous field. The power was calculated individually for each cell in the field and then summed up in order to include the heterogeneity effects. The 10 cell area in the vicinity of the inlet was excluded from the calculation.

We observe that, for each Peclet number, the power increases with $\tilde{t}$, along with the increase in heterogeneity of the field, and that is in accordance with our expectations as detailed in Section 3.1. However, if we compare the curves for different Peclet values, the observed tendency is just the opposite to the expected: while the heterogeneity of the field increases with the decrease in Peclet number, the power decreases! To explain that, we must examine closely the equation (15). Assuming that

https://doi.org/10.5194/hess-2023-84
Preprint. Discussion started: 8 May 2023

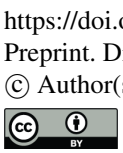

Hydrology and Earth System Sciences
Discussions
Open Access
EGU

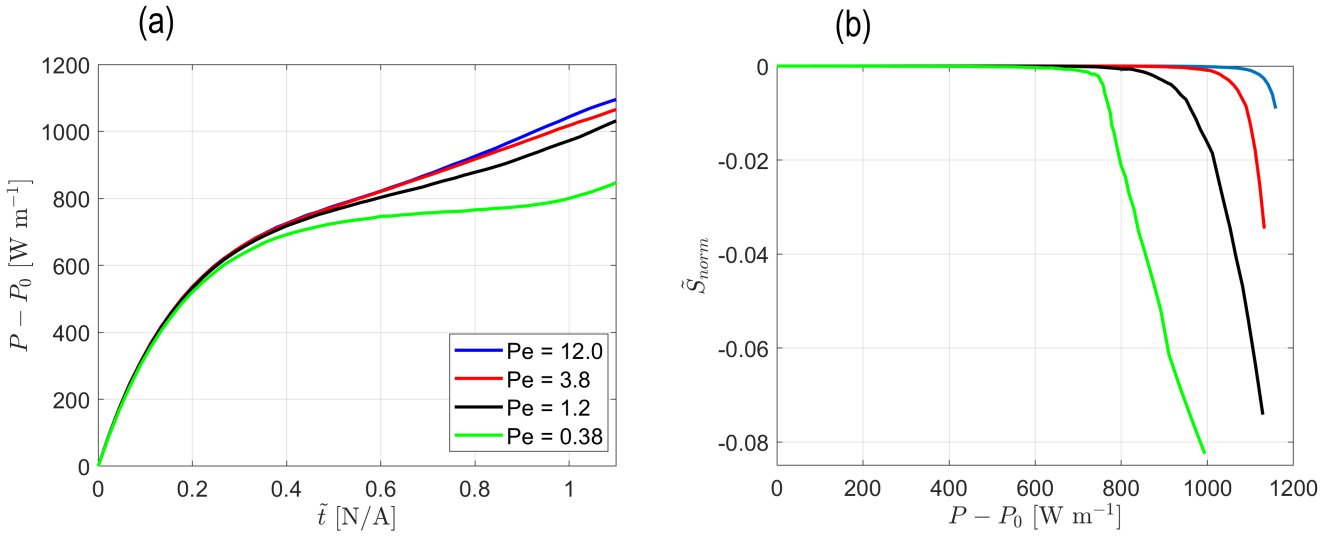

Figure 6. Hydraulic power in the field and its relation to entropy: (a) Net hydraulic power vs. dimensionless time $\tilde{t}$ and (b) Normalized mean field transport entropy $\tilde{S}_{norm}$ vs. Net hydraulic power, for different values of Peclet number.

the mean conductivity value does not change much compared to change in heterogeneity, the expression for power in a simple 1D case obtains its minimum for the completely homogeneous case and grows with the increase in heterogeneity of the field. On the other hand, power decreases with an increase in the mean conductivity value of the field (this time assuming negligible heterogeneity changes). Thus, the behavior of the net hydraulic power supplied to the flow is governed by the two opposite tendencies that result from the evolution of the coupled reactive process in the field: an increase in heterogeneity of the field, accompanied by an increase in the mean conductivity value. Finally, Figure 6c presents the normalized mean field transport entropy $\tilde{S}_{norm}$ as a function of the net hydraulic power $P - P_0$ for different values of the Peclet number. This plot shows the expected relation between the entropy of the field transport and the net hydraulic power in the field: for each Peclet number curve, the entropy of the transport in the field decreases with an increase in the net hydraulic power, reflecting an increase in transport self-organization due to an increase in power, supplied to the field in order to maintain the prescribed hydraulic pressure drop boundary condition due to an increase in the field's heterogeneity.

Following our thermodynamic framework, we thus argue that the power, required to maintain the driving head pressure drop boundary condition between inlet and outlet, increases with the increasing variance of the hydraulic conductivity in the field due to the evolution of the reactive process. This increase in power results in an increase in the level of transport self-organization in the field.

https://doi.org/10.5194/hess-2023-84
Preprint. Discussion started: 8 May 2023


Hydrology and Earth System Sciences
Discussions

5 Conclusions

Our computational study tackles the quantitative characterization of the transport self-organization that emerges in an initially homogeneous calcite porous medium due to the dynamic interaction between the reactive precipitation / dissolution processes and the solute transport. Our work leads to the following key conclusions:

- As the reactive particles advance and react in an initially homogeneous field, heterogeneity is being introduced into the field in the form of local dissolution / precipitation areas, evolving further downstream and intensifying with time. A dissolution area is located in the immediate vicinity of the inlet, where the chemical equilibrium is tilted towards dissolution; this correlates with experimental and simulation observations. The global reaction rate, normalized per unit area, is shown to be approximately constant in time. The influence of the Peclet number is exhibited by an increase in the global reaction rate with the decrease in Peclet, thus confirming that the diffusive transport mechanism, responsible for the mixing in the field, enhances reactive process. This can be explained by the fact that diffusion, being stochastic in nature, allows particles to sample regions away from the path suggested by the advection mechanism, thus allowing a better chance for reaction. The net reaction is tilted towards dissolution, as the mean conductivity value in the field grows monotonously with time, as well as with the Peclet number, which is reasonable due to the influx of low pH fluid at the inlet of the field. Similar trends are observed in the evolution of the variance of hydraulic conductivity in the field. Scalability of the field properties with the Peclet number was shown, with the mean hydraulic conductivity, conductivity variance and the global reaction rate all exhibiting dependency on the reciprocal of the Peclet number. We thus state that reactive transport scenarios for lower Peclet values, corresponding to dominant diffusive transport mechanism, coincide with an increased global reaction rate in the field and, thus, an increase in the field's heterogeneity. The dependence of the parameters that characterize the reactive process in the field on the reciprocal of the Peclet number confirms that this dimensionless number is indeed the driving force behind the evolution of the reactive process in the porous medium.
- As the reactive processes in the field advance, the evolving variations in the hydraulic conductivity of the field create an autocatalytic feedback mechanism that leads to an emergence of finger-like preferential flow paths. These paths interact, competing for the available flow, so that eventually a few paths carry the larger part of the injected particles, as seen from the increasing concentration gradients in the direction transverse to flow. This observation is confirmed by the mean normalized Shannon entropy in the field that decreases with time, signifying an increase in the level of transport self-organization in the field. The influence of the Peclet number on the evolution of transport self-organization is exhibited by a decrease in the mean normalized Shannon entropy of the transport with a decrease in Peclet, signifying an increase in self-organization. This clearly indicates that diffusion is the dominant mechanism in creating self-organization in the initially homogeneous field. Here the link between the emergence of heterogeneity and transport self-organization in an initially homogeneous field is being drawn, as the increase in heterogeneity results in the increase in the level of self-organization of the transport in the field. Peclet number scalability was shown for the mean normalized Shannon entropy curves as well. To conclude, we state that reactive transport at lower Peclet numbers, corresponding to diffusion-dominated flow, results in a higher field heterogeneity and, thus, stronger transport self-organization in the field. An

https://doi.org/10.5194/hess-2023-84
Preprint. Discussion started: 8 May 2023

important note should be made regarding the initial state of the field that undergoes reactive process: in the case of an initially homogeneous field, diffusion acts as self-organization enhancer; in an initially heterogeneous case, diffusion is capable of decreasing the transport self-organization due to its smoothing property.

- To switch the observing perspective, we turn to the particle temporal breakthrough curve in an attempt to analyze the influence of self-organization of the field's transport on the particle arrival times. The width of support of the breakthrough curves clearly increases with time, indicating an increasing scatter in non-reactive particles arrival times; this result is in line with an increase in the field's heterogeneity. A picture emerges, where the Shannon entropy of the arrival times increases with the passage of time, reflecting a larger uncertainty and a declining order in the temporal distribution of travel times. We also observe that the level of self-organization in arrival times directly correlates with the Peclet number, as the normalized breakthrough entropy decreases with increase in Peclet, an opposite tendency comparing to the entropy of the field transport. An explanation to this can be formulated in thermodynamic terms: according to the second law of Thermodynamics, the overall entropy of the system and its surroundings cannot decrease, therefore the decreasing transport entropy in the field needs to be exported to its surroundings; this is reflected in an increase of the temporal breakthrough curve entropy.

- The evolution of the reactive process in an initially homogeneous field, accompanied by the emergence of heterogeneity and, consequently, transport self-organization in the field, demands that an increased energy is supplied to the field to maintain an increasingly ordered state that emerges therein. This energy is supplied in the form of hydraulic power, required for the flow to overcome the hydraulic resistance of the porous medium. We observe that, for each Peclet number, the net hydraulic power increases with time, along with the increase in heterogeneity of the field. The decrease in power with the decrease in Peclet number, on the other hand, is due to an increase in hydraulic conductivity that accompanies the emergence of heterogeneity of the field, as explained using a simple 1D model. The entropy of the transport in the field decreases with an increase in the hydraulic power, reflecting an increase in transport self-organization. This increasing power is supplied to the field in order to maintain the hydraulic head drop boundary condition due to an increase in the field's heterogeneity. Following our thermodynamic framework, we thus argue that the power, required to maintain the driving head pressure drop boundary condition between inlet and outlet, increases with the increasing variance of the hydraulic conductivity in the field due to the evolution of the reactive process therein. This increase in the supplied power results in an increase in the level of transport self-organization in the field.

Appendix A

To illustrate how an open thermodynamic system can be maintained in a stationary nonequilibrium state through an inflow of energy, let us consider a simple heat transfer example: an open system that consists of a pair of thermal reservoirs, a hot thermal reservoir at a temperature T_h and a cold thermal reservoir at a temperature T_c, linked by heat transfer that occurs between the two reservoirs. In accordance with the second law of thermodynamics, a diffusive heat flux will occur from T_h to T_c, driven by

https://doi.org/10.5194/hess-2023-84
Preprint. Discussion started: 8 May 2023


Hydrology and Earth System Sciences
Discussions

the temperature difference of the reservoirs. In a stationary state, a constant amount of heat per unit time dQ will be removed from the hot reservoir and transferred to the cold reservoir. Recall the definition by Clausius of a change in entropy dS due to amount of heat dQ added or removed at the temperature T of the system

$$dS = \frac{dQ}{T} \tag{A.1}$$

Therefore, the entropy of a warm reservoir would decrease by dQ/T_h, whereas the entropy of a cold reservoir would increase by dQ/T_c. The net entropy change within the system is $dS = -dQ/T_h + dQ/T_c$ (notice that $dS > 0$ since $T_h > T_c$) (net entropy production within system due to irreversible heat transfer processes). In a stationary state, a constant heat flux $J = dQ/dt$ will flow through the system, resulting in the rate of internal entropy production of the system

$$\frac{dS_p}{dt} = J(\frac{1}{T_c} - \frac{1}{T_h}) > 0 \tag{A.2}$$

For the system to remain in a stationary state, its total entropy must remain constant, therefore entropy excesses have to be exported to the surroundings. In a stationary state, the rate of change of the total entropy of the system, equal to the sum of the rate of the internal entropy production in the system dS_p/dt and the rate of the entropy export to the surroundings dS_e/dt, is zero, thus

$$\frac{dS_e}{dt} = -\frac{dS_p}{dt} \tag{A.3}$$

To maintain this nonequilibrium stationary state, an energy must be invested, for example in the form of a heat pump, operating outside the system, that will transfer the heat from the cold reservoir back to the hot one in order to maintain their temperatures at constant values, otherwise the system will eventually (asymptotically) arrive at an equilibrium state. For more details on the topic of nonequilibrium thermodynamics, see Kondepudi and Prigogine (1998).

Appendix B

To acquire the basic concept of the information entropy, let us consider a single probabilistic event, having a number of possible outcomes that are assumed equally probable. For example, in case of a single symbol, transmitted in the Morse code, we have two possible outcomes (realizations) for this event - a dash and a dot (omitting the intermission between the transmitted letters). Employing the indices 0 and 1 to denote parameters before and after the event realization, initially we have $N_0 = 2$ equally possible outcomes of the message transmission event and zero initial information $I_0 = 0$. Following the transmission of a single symbol, we have a single realization of the event - a dash or a dot, thus $N_1 = 1$, and a non zero information due to the receipt of a symbol $I_1 \neq 0$.

In case of a sequence of events enumerated $1...n$, having respective number of outcomes $N_{0_1}, N_{0_2}, ..., N_{0_n}$ (consider a word that consists of n symbols in the Morse alphabet), the total number of possible outcomes is $N = N_{0_1} \cdot N_{0_2} \cdot ... \cdot N_{0_n}$. Intuitively, we would expect the information measure to be an additive parameter, so that the amount of information contained in a word

https://doi.org/10.5194/hess-2023-84
Preprint. Discussion started: 8 May 2023


Hydrology and Earth System Sciences
Discussions

transmitted with the help of the Morse code would equal to the sum of the amounts of information for each symbol that constitutes the word, that is $I(N) = I(N_{0_1} \cdot N_{0_2} \cdot ... \cdot N_{0_n}) = I(N_{0_1}) + I(N_{0_2}) + ... + I(N_{0_n})$. This can be fulfilled by choosing $I = b \ln N$, where b is a an arbitrary constant parameter, that amounts to a choice of a unit of measure (in fact, Shannon (1948) gave a formal proof that the logarithm function is the only possible relation between I and N that possesses, in addition to additivity, also continuity and monotonicity properties). For a binary system that consists of only two symbols, such as the dash and the dot in the Morse alphabet, a transmitted word of a total n symbols has $N = N_{0_1} \cdot N_{0_2} \cdot ... \cdot N_{0_n} = 2^n$ possible realizations. Taking a single transmitted symbol as one unit of information, we demand that $I = b \ln N = n$ to obtain $b = \log_2 e$ and $I = \log_2 N$. Since a single position in a sequence of symbols in a binary system is defined as a bit, the corresponding units of information I will be called $bits$ (an abbreviation from *binary digit*).

Now, assume that each of the final amount of different symbols that constitute a message has its own relative occurrence frequency (the respective probability of finding a specific symbol at a specific place in a sequence), such as the case of different letters in an alphabet. In the case of a Morse code, assume that the transmitted n-symbol word consists of n_1 dashes and n_2 dots, so that $n_1 + n_2 = n$. Using some results from combinatorics, it can be shown that

$$S = I/n = -\Sigma_i \, p_i \log_2 p_i \tag{B.1}$$

where S is the information entropy (also referred to as the Shannon entropy) per symbol and $p_i = n_i/n, \; i = 1, 2$ are the relative occurrence frequencies of both symbols. Maximum Shannon entropy obtained during the transmission of a message is when the relative occurrence frequency of each symbol is identical $p = 1/2$. It is easily shown that this maximum value equals to $S_{max} = -\log_2 p = 1$. The relation B.1 can be easily generalized for any number of possible outcomes per event.

Thus, a definition of the information entropy is obtained that possesses an additivity property, similarly to physical properties such as entropy, energy, and mass. An example that may be seen as a consequence of the results obtained with the help of the information theory is that in modern communication methods the more common alphabet letters are encoded in such a way that their information content is minimized in order to facilitate the transmission process. Thus, in a Morse code a letter E is encoded by a single dot, while J is a dot followed by three dashes. For more details on the topic of Shannon entropy, see Shannon (1948).

Code and data availability. A dedicated repository, containing all codes and data, will be created on GitHub.

Author contributions. ES developed the research methodology, wrote major parts of the simulation code, performed numerical simulations, analyzed data, and wrote the manuscript. YE supervised the implementation of the research methodology, supplied the initial version of the simulation code, and oversaw the writing of the manuscript.

https://doi.org/10.5194/hess-2023-84
Preprint. Discussion started: 8 May 2023

Competing interests. The authors have no competing interests to declare.

Acknowledgements. Y.E. and E.S. thank the support of the Israel Science Foundation (grant No.801/20).

https://doi.org/10.5194/hess-2023-84
Preprint. Discussion started: 8 May 2023

References

Ajayi, T., Gomes, J. S., and Bera, A.: A review of CO2 storage in geological formations emphasizing modeling, monitoring and capacity estimation approaches, Water Resources research, 50, 1490–1505, https://doi.org/https://doi.org/10.1002/2013WR015111, 2014.

Al-Khulaifi, Y., Lin, Q., Blunt, M. J., and Bijeljic, B.: Reaction Rates in Chemically Heterogeneous Rock: Coupled Impact of Structure and Flow Properties Studied by X-ray Microtomography, Environmental Science Technology, 51(7), 4108–4116, https://doi.org/https://doi.org/10.1021/acs.est.6b06224, 2017.

Ben-Naim, A.: A Farewell to Entropy, WORLD SCIENTIFIC, https://doi.org/10.1142/6469, 2008.

Berkowitz, B. and Zehe, E.: Surface water and groundwater: unifying conceptualization and quantification of the two "water worlds", Hydrology and Earth System Sciences, 24, 1831–1858, https://doi.org/https://doi.org/10.5194/hess-24-1831-2020, 2020.

Berkowitz, Y., Edery, Y., Scher, H., and Berkowitz, B.: Fickian and non-Fickian diffusion with bimolecular reactions, Phys. Rev. E, 87, 032 812, https://doi.org/10.1103/PhysRevE.87.032812, 2013.

Beven, K. and Germann, P.: Macropores and Water Flow in Soils, Water Resources Research - WATER RESOUR RES, 18, 1311–1325, https://doi.org/10.1029/WR018i005p01311, 1982.

Borgne, T. L., Dentz, M., and Ramírez, J. C.: Lagrangian Statistical Model for Transport in Highly Heterogeneous Velocity Fields, Physical Review Letters, 101, 090 601, https://doi.org/DOI:10.1103/PhysRevLett.101.090601, 2008.

Brusseau, M. L.: Transport of reactive contaminants in heterogeneous porous media, Reviews of Geophysics, 32, 285–313, https://doi.org/https://doi.org/10.1029/94RG00624, 1994.

Camazine, S., Deneubourg, J.-L., Franks, N. R., Sneyd, J., Theraula, G., and Bonabeau, E.: Self-Organization in Biological Systems, Princeton University Press, 2001.

Chiogna, G. and Rolle, M.: Entropy-based critical reaction time for mixing-controlled reactive transport, Water Resources Research, 53, 7488–7498, https://doi.org/https://doi.org/10.1002/2017WR020522, 2017.

Clausius, R.: Uber die Art der Bewegung, welche wir Warme nennen, Annalen der Physik und Chemie, 79, 353–380, 1857.

Deng, H., Poonoosamy, J., and Molins, S.: A reactive transport modeling perspective on the dynamics of interface-coupled dissolution-precipitation, Applied Geochemistry, 137, 105 207, https://doi.org/https://doi.org/10.1016/j.apgeochem.2022.105207, 2022.

Domenico, P. A. and Schwartz, F. W.: Physical and Chemical Hydrogeology, 2nd Edition, John Wiley & sons Ltd., 1997.

Edery, Y., Scher, H., and Berkowitz, B.: Modeling bimolecular reactions and transport in porous media, Geophysical Research Letters, 36, https://doi.org/https://doi.org/10.1029/2008GL036381, 2009.

Edery, Y., Scher, H., and Berkowitz, B.: Particle tracking model of bimolecular reactive transport in porous media, Water Resources Research, 46, https://doi.org/https://doi.org/10.1029/2009WR009017, 2010.

Edery, Y., Scher, H., and Berkowitz, B.: Dissolution and precipitation dynamics during dedolomitization, Water Resources Research, 47, https://doi.org/https://doi.org/10.1029/2011WR010551, 2011.

Edery, Y., Guadagnini, A., Scher, H., and Berkowitz, B.: Reactive transport in disordered media: Role of fluctuations in interpretation of laboratory experiments, Advances in Water Resources, 51, 86–103, https://doi.org/https://doi.org/10.1016/j.advwatres.2011.12.008, 35th Year Anniversary Issue, 2013.

Edery, Y., Guadagnini, A., Scher, H., and Berkowitz, B.: Origins of anomalous transport in heterogeneous media:Structural and dynamic controls, Physical Review, 99, https://doi.org/https://doi.org/10.1103/PhysRevE.99.033108, 2014.

https://doi.org/10.5194/hess-2023-84
Preprint. Discussion started: 8 May 2023

Edery, Y., Geiger, S., and Berkowitz, B.: Structural controls on anomalous transport in fractured porous rock, Water Resources Research, 52, 5634–5643, https://doi.org/https://doi.org/10.1002/2016WR018942, 2016a.

Edery, Y., Porta, G., Guadagnini, A., Scher, H., and Berkowitz, B.: Characterization of Bimolecular Reactive Transport in Heterogeneous Porous Media, Transport in Porous Media, 115, 291–310, https://doi.org/https://doi.org/10.1007/s11242-016-0684-0, 2016b.

Edery, Y., Stolar, M., Porta, G., and Guadagnini, A.: Feedback mechanisms between precipitation and dissolution reactions across randomly heterogeneous conductivity fields, Hydrol. Earth Syst. Sci., pp. 5905—-5915, https://doi.org/https://doi.org/10.5194/hess-25-5905-2021, 2021.

Guadagnini, A. and Neuman, S. P.: Nonlocal and localized analyses of conditional mean steady state flow in bounded, randomly nonuniform domains: 1. Theory and computational approach, Water Resources Research, 35, 2999–3018, https://doi.org/https://doi.org/10.1029/1999WR900160, 1999.

Haken, H.: Synergetics : an introduction: nonequilibrium phase transitions and self-organization in physics, chemistry, Springer series in synergetics, v.1, Springer-Verlag Berlin Heidelberg, 1983.

Hemelrijk, C. K. and Hildenbrandt, H.: Schools of fish and flocks of birds: their shape and internal structure by self-organization, Interface Focus, 2, https://doi.org/https://doi.org/10.1098/rsfs.2012.0025, 2012.

Jiao, T., Ye, M., Jin, M., and Yang, J.: A finite particle method (FPM) for Lagrangian simulation of conservative solute transport in heterogeneous porous media, Advances in Water Resources, 156, 104 043, https://doi.org/https://doi.org/10.1016/j.advwatres.2021.104043, 2021.

Kamolpornwijita, W., Liangb, L., Westa, O., Molinea, G., and Sullivan, A.: Preferential flow path development and its influence on long-term PRB performance: column study, Journal of Contaminant Hydrology, 66, 161–178, https://doi.org/https://doi.org/10.1016/S0169-7722(03)00031-7, 2003.

Kloeden, P. E.: Numerical solution of stochastic differential equations, Applications of mathematics; v. 23, Springer, Berlin, 1992.

Kondepudi, D. and Prigogine, I.: Modern Thermodynamics: From Heat Engines to Dissipative Structures, John Wiley & sons Ltd., 1998.

Ladd, A. and Szymczak, P.: Reactive Flows in Porous Media: Challenges in Theoretical and Numerical Methods, Annual Review of Chemical and Biomolecular Engineering, 12, 543–571, https://doi.org/10.1146/annurev-chembioeng-092920-102703, 2021.

Leone, F. C., Nelson, L. S., and Nottingham, R. B.: The Folded Normal Distribution, Technometrics, 3, 543–550, https://doi.org/10.1080/00401706.1961.10489974, 1961.

Li, W., Einstein, H. H., and Germaine, J. T.: An Experimental Study of Matrix Dissolution and Wormhole Formation Using Gypsum Core Flood Tests: 1. Permeability Evolution and Wormhole Geometry Analysis, Journal of Geophysical Research: Solid Earth, 124, https://doi.org/https://doi.org/10.1029/2018JB017238, 2019.

Manahan, S.: Environmental Chemistry, 9th ed., CRC Press, 2000.

Mays, D. C., Faybishenko, B. A., and Finsterle, S.: Information entropy to measure temporal and spatial complexity of unsaturated flow in heterogeneous media, Water Resources Research, 38, https://doi.org/https://doi.org/10.1029/2001WR001185, 2002.

Meakin, P. and Tartakovsky, A. M.: Modeling and simulation of pore-scale multiphase fluid flow and reactive transport in fractured and porous media, Reviews of Geophysics, 47, https://doi.org/https://doi.org/10.1029/2008RG000263, 2009.

Morse, J. and Mackenzie, F.: Geochemistry of Sedimentary Carbonates, Vol. 48, 1st Edition, Developments in Sedimentology, Elsevier Science, 1990.

Nguyen, V. and Papavassiliou, D. V.: Hydrodynamic Dispersion in Porous Media and the Significance of Lagrangian Time and Space Scales, Geochimica et Cosmochimica Acta, 5, https://doi.org/https://doi.org/10.3390/fluids5020079, 2020.

https://doi.org/10.5194/hess-2023-84
Preprint. Discussion started: 8 May 2023

Nissan, A. and Berkowitz, B.: Reactive Transport in Heterogeneous Porous Media Under Different Péclet Numbers, Water Resources Research, 55, https://doi.org/https://doi.org/10.1029/2019WR025585, 2019.

Perez, L. J., Hidalgo, J. J., and Dentz, M.: Reactive Random Walk Particle Tracking and Its Equivalence With the Advection-Diffusion-Reaction Equation, Water Resources Research, 55, 847–855, https://doi.org/https://doi.org/10.1029/2018WR023560, 2019.

Petrosino, F., Rosa, D. D., and Mingione, G.: Application of different Lagrangian Particle Tracking techniques for water impingement, IOP Conference Series: Materials Science and Engineering, 1024, 012 011, https://doi.org/10.1088/1757-899X/1024/1/012011, 2021.

Poonoosamy, J., Klinkenberg, M., Deissmann, G., Brandt, F., Bosbach, D., Mäder, U., and Kosakowski, G.: Effects of solution supersaturation on barite precipitation in porous media and consequences on permeability: Experiments and modelling, Geochimica et Cosmochimica Acta, 270, 43–60, https://doi.org/https://doi.org/10.1016/j.gca.2019.11.018, 2020.

Radolinski, J., Le, H., Hilaire, S. S., Xia, K., Scott, D., and Stewart, R. D.: A spectrum of preferential flow alters solute mobility in soils, Scientific Reports, 12, https://doi.org/https://doi.org/10.1038/s41598-022-08241-w, 2022.

Risken, H.: The Fokker-Planck Equation: Methods of Solution and Applications, Springer Series in Synergetics, Springer Berlin Heidelberg, 1996.

Schmidt, M. J., Pankavich, S. D., Navarre-Sitchler, A., and Benson, D. A.: A Lagrangian method for reactive transport with solid/aqueous chemical phase interaction, Journal of Computational Physics: X, 2, 100 021, https://doi.org/https://doi.org/10.1016/j.jcpx.2019.100021, 2019.

Schrodinger, E.: What is Life?: With Mind and Matter and Autobiographical Sketches, Cambridge University Press, 1944.

Schweizer, D., Blum, P., and Butscher, C.: Uncertainty assessment in 3-D geological models of increasing complexity, Solid Earth, 8, 515–530, https://doi.org/https://doi.org/10.5194/se-8-515-2017, 2017.

Shannon, C. E.: A Mathematical Theory Of Communication, Bell System Technical Journal, 782, 623–656, https://doi.org/https://doi.org/10.1002/j.1538-7305.1948.tb01338.x, 1948.

Shazly, A. E.: Acid Gas Injection into Petroleum Reservoirs: A Review, Petroleum and Petrochemical Engineering Journal, 5, https://doi.org/https://doi.org/10.23880/ppej-16000280, 2021.

Shirolkar, J., Coimbra, C., and Queiroz McQuay, M.: Fundamental aspects of modeling turbulent particle dispersion in dilute flows, Progress in Energy and Combustion Science, 22, 363–399, https://doi.org/https://doi.org/10.1016/S0360-1285(96)00006-8, 1996.

Singurindy, O. and Berkowitz, B.: Flow, Dissolution and Precipitation in Dolomite, Water Resources Research, 39, https://doi.org/https://doi.org/10.1029/2002WR001624, 2003.

Snippe, J., Berg, S., Ganga, K., Brussee, N., and Gdanski, R.: Experimental and numerical investigation of wormholing during CO2 storage and water alternating gas injection, International Journal of Greenhouse Gas Control, 94, https://doi.org/https://doi.org/10.1016/j.ijggc.2019.102901, 2020.

Sole-Mari, G. and Fernandez-Garcia, D.: Lagrangian Modeling of Reactive Transport in Heterogeneous Porous Media With an Automatic Locally Adaptive Particle Support Volume, Water Resources Research, 54, 8309–8331, https://doi.org/https://doi.org/10.1029/2018WR023033, 2018.

Sole-Mari, G., Fernàndez-Garcia, D., Sanchez-Vila, X., and Bolster, D.: Lagrangian Modeling of Mixing-Limited Reactive Transport in Porous Media: Multirate Interaction by Exchange With the Mean, Water Resources Research, 56, e2019WR026 993, https://doi.org/https://doi.org/10.1029/2019WR026993, 2020.

Stamm, C., Flühler, H., René, G., Leuenberger, J., and Wunderli, H.: Preferential Transport of Phosphorus in Drained Grassland Soils, Journal of Environmental Quality - J ENVIRON QUAL, 27, https://doi.org/10.2134/jeq1998.00472425002700030006x, 1998.

https://doi.org/10.5194/hess-2023-84
Preprint. Discussion started: 8 May 2023

Stolum, H.: River Meandering as a Self-Organization Process, Science, 271, 1710–1713, https://doi.org/10.1126/science.271.5256.1710, 1996.

Szymczak, P. and Ladd, A.: A network model of channel competition in fracture dissolution, Geophysical Research Letters, 33, https://doi.org/https://doi.org/10.1029/2005GL025334, 2006.

Turing, A. M.: The Chemical Basis of Morphogenesis, Philosophical Transactions of the Royal Society of London. Series B, Biological Sciences, 237, 37–72, https://doi.org/https://doi.org/10.1098/rstb.1952.0012, 1952.

Woodbury, A. D. and Ulrych, T. J.: Minimum relative entropy inversion: Theory and application to recovering the release history of a groundwater contaminant, Water Resources Research, 32, 2671–2681, https://doi.org/https://doi.org/0043-1397/96/95WR-03818509.00, 1996.

Yan, X., Sun, Z., Li, S., Yang, W., and Zhang, Y.: Evaluation of Effectiveness of CO2 Sequestration Using Portland Cement in Geological Reservoir Based on Unified Pipe-network Method, Energies, 13, https://doi.org/https://doi.org/10.3390/en13020387, 2020.

Zehe, E., Loritz, R., Edery, Y., and Berkowitz, B.: Preferential Pathways for Fluid and Solutes in Heterogeneous Groundwater Systems: Self-Organization, Entropy, Work, Hydrol. Earth Syst. Sci., 25, 5337–5353, https://doi.org/https://doi.org/10.5194/hess-25-5337-2021, 2021.

Zhang, Y., Cao, Z., Hou, F., and Cheng, J.: Characterizing Preferential Flow Paths in Texturally Similar Soils under Different Land Uses by Combining Drainage and Dye-Staining Methods, Water, 13, https://doi.org/https://doi.org/10.3390/w13020219, 2021.

Zhang, Z. and Chen, Q.: Comparison of the Eulerian and Lagrangian methods for predicting particle transport in enclosed spaces, Atmospheric Environment, 41, 5236–5248, https://doi.org/https://doi.org/10.1016/j.atmosenv.2006.05.086, 2007.